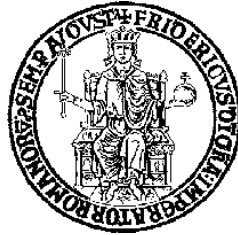


UNIVERSITA' DEGLI STUDI DI NAPOLI FEDERICO II



DEPARTMENT OF INDUSTRIAL ENGINEERING

**PH.D. THESIS IN AEROSPACE, MARINE AND QUALITY
ENGINEERING**

**HYDRODYNAMIC AND STRUCTURAL
CORRELATIONS FOR THE WATER IMPACT OF
HIGH SPEED PLANING CRAFT**

Tutors:

Prof. Sergio De Rosa

Prof. Francesco Franco

Prof.ssa Ermina Begovic

Prof. Carlo Bertorello

Chairman:

Prof. Luigi de Luca

Candidate:

Ing. Nicola Santoro

UNIVERSITA' DEGLI STUDI DI NAPOLI FEDERICO II



DEPARTMENT OF INDUSTRIAL ENGINEERING



PH.D. THESIS IN AEROSPACE, MARINE AND QUALITY ENGINEERING

**HYDRODYNAMIC AND STRUCTURAL
CORRELATIONS FOR THE WATER IMPACT OF
HIGH SPEED PLANING CRAFT**

Tutors:

Prof. Sergio De Rosa

Prof. Francesco Franco

Prof.ssa Ermina Begovic

Prof. Carlo Bertorello

Chairman:

Prof. Luigi De Luca

Candidate:

Ing. Nicola Santoro

Preface

The analysis of the water impact of a rigid body finds a lot of applications in different engineering fields: civil, mechanical, aeronautical, naval, etc.

For instance, in civil engineering the problem is for the bridge pillars into a river, in the aerospace field the airplane or helicopters sea landing is widely studied phenomenon and so on for the other engineering phenomena.

One of the most important applications can be found in naval field, where the slamming phenomenon is widely studied for the high stress caused on the structure.

The analytical formulation of the slamming phenomenon has been studied by different authors, following both 2D and 3D approaches. Of course, the second one, with 3D geometry and forward speed with incident waves, takes into account more effects than 2D theories, but it complicates the impact analysis to a situation that does not seem feasible to easily solve by numerical methods at moment.

Thus, this work is focused on the theoretical 2D formulation, useful to have a prediction before the direct measurements of the pressure through a wide experimental campaign.

This thesis characterizes the dynamic water impact for the high speed planing craft and the hydrodynamic and structural correlations, between different sizes of models, are implemented.

In literature, the analytical and the experimental studies of the water impact problem have been analysed looking only to a single impact into water, neglecting the craft forward speed, the trim angle, the air incursion and other effects; so, the peculiarity of this work is that, the time history of a run, with various impacts, is studied, in order to have a

complete frequency analysis, useful to characterize the dynamic structural behaviour of the hull bottom panels.

Introduction

In the marine field, the water impact of the bow is usually called slamming. This phenomenon is different for low speed vessels (Figure 1.1) and high speed planing craft (Figure 1.2); in the first case the slamming is a rare event and the study of it could be treated by a statistical approach, for the second case the slamming phenomenon is defined as the re-entry into water after the craft becomes partially airborne; this is a periodic event and the study of it should be done following a deterministic approach both in time and frequency domain.



Figure 1.1: Slamming for low speed vessels



Figure 1.2: Slamming for high speed planing craft

The slamming pressure assessment is an important topic for shell plating and stiffener design of bow flare.

In the first part of this work, the pressure distribution on the bottom plating of a high speed planing craft is evaluated through measurements of the impact pressures on scale model running in regular waves.

The planing hull model is a monohedral hard chine, built with clear bottom and deck, in order to allow the visual inspection of the fluid flow and the exact points of impact. It has been extensively studied in previous works.

From the time histories of vertical motions (heave and pitch) and bow acceleration of the model measured in “standard” seakeeping tests, preliminary assessment of the slamming impact pressure according to Zhao and Faltinsen (2005) method is performed. The experimental campaign presented in this first part is focused on the pressure field assessment in nine points of the hull bottom surface running at four velocities and two regular waves. Results analysis in time and frequency domain is given, identifying the pressure distribution along the bottom panel. Furthermore, comparison of measured, analytical and normative values has been performed.

In the second part of the thesis, after the hydrodynamic phenomenon analysis, the elastic behaviour of different bottom panels is predicted.

In order to study a real case, after the scantlings of a real planing craft bottom panels, with four different materials, an analytical and numerical modal analysis is performed and a scaling method is implemented, in order to obtain the scale panels with the same structural dynamic behaviour.

As final step, a preliminary dynamic analysis of the panels, under the hydrodynamic load, is performed; this has been done in order to analyse which characteristic structural natural frequencies are more

excited and if this behaviour is well correlated with full scale. It is useful to see which panels characteristic frequencies are more excited and the maximum displacement of the panels, because it is possible to have an indication about which frequencies to avoid due to machinery equipment (engine, shaft, generators, etc.).

TABLE OF CONTENTS

1.STATE OF ART.....	17
1.1 Dynamic impact	17
1.2 Slamming.....	18
1.2.1 Water entry problem	18
1.3 Similitude	21
1.4 Experimental methods and scaling laws for water impact	22
2.HYDRODYNAMIC AND IMPACT PRESSURE PREDICTION.....	25
2.1 Water impact on rigid bodies	25
2.2 Experimental set-up.....	28
2.3 Seakeeping tests and pressure evaluation.....	30
3.HYDRODYNAMIC AND IMPACT PRESSURE MEASUREMENT	35
3.1 Experimental set-up and instruments	35
3.2 Experimental tests results and analysis	37
3.2.1 Pressure values	37
3.2.2 Analysis in the frequency domain.....	46
3.2.3 Results comparison	50
4.PRELIMINARY INVESTIGATION ON THE DYNAMIC BEHAVIOUR OF DIFFERENT BOTTOM PANELS.....	53
4.1 Scantlings of full scale bottom panels.....	53
4.2 Modal analysis and scantlings of the panels	55
4.3 Preliminary dynamic analysis of the panels under the hydrodynamic load	59

4.3.1	Hydrodynamic load definition	60
4.3.2	Dynamic analysis results.....	60
5.	CONCLUSIONS	65
APPENDIX A	67
Part I	67
Part II	83
APPENDIX B	87
PART I	87
Part II	94
6.	ACKNOWLEDGMENTS	97
Bibliography	99

Tables of Figures

Figure 1.1: Slamming for low speed vessels	7
Figure 1.2: Slamming for high speed planing craft	7
Figure 2.1: von Karman wedge	25
Figure 2.2: Wagner wedge	27
Figure 2.3: Experimental set-up	29
Figure 2.4: Amplitude of vertical motions at bow	30
Figure 2.5: Vertical accelerations at bow	31
Figure 2.6: Predictions of pressure (p) distribution during water entry of a rigid wedge with constant vertical velocity V	31
Figure 2.7: Zhao and Falinsen diagram of hydrodynamic pressure distribution.....	32
Figure 2.8: : Comparison between predicted pressure trend for three forward speed.....	33
Figure 3.1: Pressure sensor model EPX-N02-1,5B-/Z2.....	35
Figure 3.2: Static calibration system	36
Figure 3.3: Sensor position.....	36
Figure 3.4: Main measured values during a run at forward speed of 6.32 m/s	38
Figure 3.5: Pressure trend for positions (a) A1 A2 A3, (b) B1 B2 B3 and (c) C1 C2 C3 at model speed 6.32 m/s.....	40
Figure 3.6: Characteristic values $p_{1/3}$, $p_{1/10}$ and p_{mean} of the pressure peaks, at point A1, in function of forward speed.....	41
Figure 3.7: Characteristic values $p_{1/3}$, $p_{1/10}$ and p_{mean} of the pressure peaks, at point A2, in function of forward speed.....	41
Figure 3.8: Characteristic values $p_{1/3}$, $p_{1/10}$ and p_{mean} of the pressure peaks, at point A3, in function of forward speed.....	41
Figure 3.9: Pressure field at $v = 3.4$ and 4.6 m/s	42
Figure 3.10: Pressure field at $v = 5.57$ and 6.32 m/s	43
Figure 3.11: Impact pressure mean values for the longitudinal position A1, A2 and A3	44
Figure 3.12: Impact pressure mean values in point A1.....	45
Figure 3.13: Single peak of pressure for test condition 4 at position A1	46
Figure 3.14: Transfer from time to frequency domain	47
Figure 3.15: Pressure FFT for points A1, A2, A3 at model speed 6.32 m/s	48
Figure 3.16: FFT of vertical acceleration and encounter wave amplitude at model speed 6.32 m/s.....	48
Figure 3.17: Cross-correlation analysis between pressure, acceleration and wave at point A2 at model speed of 6.32 m/s.....	49
Figure 3.18: Comparison between measured and analytical hydrodynamic pressure at point A1	50
Figure 4.1: Full-scale craft Gagliotta 44.....	53
Figure 4.2: Structures plan of the full-scale craft	54
Figure 4.3: (a) mode 1, (b) mode 2 and (c) mode 3 of composite scale panels.....	59

Figure 4.4: Glass fiber composite panel dynamic response at model speed of 5.53 m/s61
Figure 4.5: Glass-kevlar fiber composite panel dynamic response at model speed of 5.53 m/s61
Figure 4.6: Carbon fiber composite panel dynamic response at model speed of 5.53 m/s62
Figure 4.7: Aluminium panel dynamic response at model speed of 5.53 m/s.....62

List of Tables

Table 2.1: Model characteristics.....	29
Table 2.2: Seakeeping test conditions	30
Table 2.3: Zhao and Faltinsen slamming parameters	32
Table 3.1: Test conditions for pressure measurements	37
Table 3.2: Pressure sensors positions	37
Table 3.3: Scheme of the scale-down method	50
Table 4.1: Full-scale glass fiber composite and aluminium panels characteristics	54
Table 4.2: Full-scale kevlar-glass fiber and carbon fiber composite panels characteristics.....	54
Table 4.3: Natural frequencies for full-scale glass fiber composite panel and aluminium panel.....	56
Table 4.4: Natural frequencies for full-scale kevlar-glass fiber and carbon fiber composite panels.....	56
Table 4.5: Model scale glass fiber composite and aluminium panels characteristics	57
Table 4.6: Model scale kevlar-glass fiber and carbon fiber composite panels characteristics	58
Table 4.7: Natural frequencies for scale glass fiber composite panel and aluminium panel.....	58
Table 4.8: Natural frequencies for scale kevlar-glass fiber and carbon fiber composite panels	58

1. STATE OF ART

1.1 Dynamic impact

Before approaching the central topic of this thesis, in the first part of this chapter, the state of art of dynamic impact is briefly introduced.

Most of the structural problems are often studied through static or quasi-static approaches and the effect of inertia are neglected. The analysis of dynamic impact, especially on composite materials, is mentioned below.

In a paper by A. S. Yigit and A. P. Christoforou [1], the dynamics of composite beam subject to transverse impact is investigated. A linearized contact law based on an elastic-plastic contact is shown to yield excellent results for impact response. A dynamic ratio is used to characterize the type of impact response, i.e. whether it is locally dominated, quasi-static or dynamic. This ratio is defined as the ratio of the maximum impact force, obtained from the dynamic simulation, compared to the one obtained from a half-space analysis (i.e. local contact).. It is found that this depends on a single dimensionless parameter called "dynamic impact number", which also governs the initial impact response until the waves are reflected back from the boundaries. The contact models used in most impact studies are traditionally based on the Hertzian contact law [2-4].

Qiao and Yang, in their studies [5, 6], analyse the behaviour of fiber reinforced polymer honeycomb and soft-core composite sandwich beams. In these studies a higher-order impact model is presented to simulate the response of sandwich beam subjected to a foreign impact. The predicted impact responses (e.g. contact force and central deflection) are compared with the finite elements simulation by LS-DYNA. The presented impact analysis demonstrates the accuracy and

capability of the higher-order impact sandwich beam theory, it can be used effectively in analysis, design applications and optimization of efficient sandwich structures for impact protection and mitigation.

1.2 Slamming

Approaching the study of the dynamic impact, the attention has been focused on the marine field and on the most common dynamic impact which occurs against the naval structures: the *slamming*.

Slamming is defined as the re-entry into water of the ship's bow. This phenomenon is different for high speed planing craft and low speed vessels. In the first case the impact on the water is periodic; for the second case, the slamming is a rare event and the study of it could be treated by a statistical approach.

Assessment of slamming pressures is important in designing plates and stiffeners in bow flare, bottom, and possibility flat stern areas of ships and in the cross structure (wetdeck) of multihulls. Design slamming pressures are usually obtained by using formulae given by the classification societies. However, these formulae are fully empirical and therefore not necessarily valid and thus suitable for novel designs. Therefore, there is a growing need for direct calculation methods.

1.2.1 Water entry problem

According with the pioneering works by von Karman [7] and Wagner [8], the pressure determination in impact problems is simplified to the water entry of a two-dimensional section of a hull (wedge analogy) with different levels of mathematical accuracy. Zhao (et al.) [9, 10], Faltinsen [11] and Lewis (et al.) [12]. Zhao and Faltinsen present two different theoretical methods for predicting slamming loads on two-dimensional sections. One of the methods [9] (developed in 1993) is a

fully non-linear numerical simulation, that includes flow separation from knuckles or fixed separation points of a body with continuously curved surface. The other method (1997) [10] present a "generalized Wagner theory" that is a simplification of the exact solution of the water entry problem, already presented in [9], and it is an approximate solution; it does not include the flow separation. "Generalized Wagner theory" means that the exact boundary conditions are satisfied. All terms in Bernoulli's equation are included (as shown below) except the hydrostatic pressure term. If the predicted pressure becomes less than the atmospheric pressure, p_a , the pressure is simply set equal to this latter. This occurs at the spray root and is caused by the square-velocity term in Bernoulli's equation.

In their works A. Carcaterra and E. Ciappi [13, 14], provide a theoretical and experimental analysis of the response of an elastic system carried on board a wedge-shaped body impacting the water surface.

Other analytical methods are available from the literature to assess slamming pressure [15].

Some numerical studies of this phenomenon can be also found; Hermundstad and Moan in [16, 17] present an efficient numerical method and applied it to a passengers vessel at Froude number around 0.3 in head and oblique seas. They distinguish two main approaches, namely the "k-factor methods" and the "direct methods". The k-factors methods are based on the use of slamming coefficients or so-called k-factors; these k-factors relate the slamming pressure to the square of the impact velocity, and they can be calculated, or obtained experimentally, prior to the ship motion analysis. In a direct method, one starts out with the ship motion calculations, and then applies the slamming calculation method each time a slamming event takes place.

I. Stenius and A. Rosén [18] consider finite element modelling of the hydrodynamic loads in hull-water impacts. The aim of that work is to investigate the modelling of hydrodynamic impact loads by use of the explicit FE-code LS-DYNA. In another study [19], this software is used; K. Das and R. C. Batra analyse the local water slamming referred to the impact of a part of a ship hull on stationary water for a short duration, during which high local pressures occur on the hull. They simulate slamming impact of rigid and deformable hull bottom panels by using the Lagrangian and Eulerian formulations included in the software LS-DYNA. The great advantage of this modelling technique is that it enables the modelling of instantaneous fluid-structure interaction. In heavy sea, slamming and wave impact are observed by Mizoguchi and Tanizawa [20]. These wave loads are of practical importance for naval architecture to design a safety ship operator to carry cargoes in safety. In this review section, the principle phenomenon and the prediction methods of these wave loads are presented. These include theories of slamming impact both of Wagner type and Bagnold type and application of numerical simulation methods to the slamming impact. Further they also analyse the elastic response of ship structures to slamming impact loads and long-term prediction theories of slamming impact loads and the elastic response. In 2008 S. Kim and D. Novak [21] present the developments at ABS to revise the requirements for slamming impact loads on high speed naval craft. According to the ABS Guide for Building and Classing High Speed Naval Craft (HSNC 2007), slamming impact load is one of the most critical factors for the scantling design of hull structures. Extensive numerical simulations are carried out using the non-linear time domain seakeeping program LAMP. This paper also presents ABS's on-going efforts for the development and validation of computational fluid dynamics (CFD)

code as an alternative numerical tool to analyse the extremely violent non linear free-surface flows such as, sloshing, slamming and green water impact problem.

Mark Battley, [22], describes a dynamic finite elements analysis based study of slamming impacts on marine composites panel structures; he shows that the response is highly dependent on the impact velocity, dead-rise angle, natural frequency of the panel and the frequency content of the loading

1.3 Similitude

After understanding the analytical theory of a phenomenon, of course, any new design is extensively evaluated experimentally until it achieves the necessary reliability, performance and safety. However, the experimental evaluation of a structures is costly and time consuming. Consequently, it is extremely useful if a full-scale structure can be replaced by a similar (scaled-down) model, which is much easier to be used. Furthermore, a dramatic reduction in cost and time can be achieved, if available experimental data of a specific structure can be used to predict the behaviour of a group of similar system.

Similitude theory is thus employed to develop the necessary similarity conditions (scaling laws). Scaling laws provide relationship between a full-scale structure and its scale model, and can be used to extrapolate the experimental data of a small, inexpensive and testable model into design information for a large prototype. There are two methods to develop similarity conditions, the direct use of governing equations and dimensional analysis. The similarity conditions can be established either directly from the field equations of the system or, if it is a new phenomenon and the mathematical model of the system is not available, through dimensional analysis. The first method is more convenient than

dimensional analysis, since the resulting similarity conditions are more specific. In fact, in this case, the field equations of the system with proper boundary and initial conditions characterize the behaviour of the system in terms of its variables and parameters. Examples of the direct use of governing equations is offered by Simitse [23, 24]: only direct use of the governing equations procedure is considered. If the field equations of the scale model and its prototype are invariant under the transformation, then the two systems are completely similar. This transformation defines the scaling laws among all parameters belonging to the two systems.

By using dimensional analysis [25-28], an incomplete form of the characteristic equation of the system can be formulated. This equation is in terms of dimensionless products of variables and parameters of the system. Then, similarity conditions can be established on the basis of this equation.

1.4 Experimental methods and scaling laws for water impact

The scaling laws and the related similitude can be applied to a lot of physical phenomena and engineering problems. In literature it is also possible to find several applications.

In the marine field the most common application of scaling laws is for performance prediction of ship models using Froude method. Furthermore, also for the experimental study of the hydrodynamic impact, caused by slamming, is useful to apply a similitude method. In the studies by Lee and Wilson [29] and Manganelli [30], pressure transducers and a special measurement system named "Slam Patch" have been designed and implemented to measure the hydro-impact pressure and/or the local structure's response. The measurement systems are installed on a 1/7-scale model of an Open 60 yacht. Modal,

rotational drop and seakeeping-slamming tests are carried out. The measured hydro-impact pressure is processed statistically. A methodology to scale up the test results to prototype is mentioned (force by λ^3 , pressure by λ , time by $\lambda^{1/2}$, quantity of force impulse by $\lambda^{7/2}$, quantity of pressure impulse by $\lambda^{3/2}$). At the same time, the transient response of a simple structure under half-sine impulse is calculated using a commercial finite element analysis program to study the effect of the relationship between impulse duration and natural frequency of the structure.

Other experimental studies were been done by M. Battley; in [31] experimental measurements of transient strains, local acceleration and pressure are undertaken on the IMOCA Open 60' class sailing yacht, and on a replica hull panel section tested in a laboratory slam testing facility; the testing facility used in this study is known as the Servo-hydraulic Slam Testing System (SSTS).

In other papers Battley describes the use of SSTS to test impact of marine sandwich panels [32, 33] and of composite hull panels [34] with water. In fact the sandwich panels are widely used within the marine industry, particularly as primary hull shell structure, but also as appendages and deck housing. Hydrodynamic loads can be very significant for these structures, particularly for high-speed craft.

One of the most important experimental studies about planing pressure is developed by Garne [35, 36], he describes an experimental study with the major aim to get a detailed picture of the pressure distribution carrying a planing craft at high speed through calm water and waves. The instrumentation, load cases and performed runs are discussed as well as the steps to use the measurement data for evaluation of numerical models for planing craft in waves.

Other relevant studies concerning the analytical/experimental analysis about slamming impact are in [37, 38], which characterize slamming loads acting on fast monohull vessels.

In the next sections an experimental campaign on an high speed planing craft in regular waves is presented, in order to measure and to analyse the hydrodynamic and impact pressure; furthermore, an analysis of the elastic behaviour of four different bottom panels is developed.

2. HYDRODYNAMIC AND IMPACT PRESSURE PREDICTION

2.1 Water impact on rigid bodies

To study the water impact phenomenon, the body can be assumed rigid in the hydrodynamic calculations. Several approximations can be made in the analysis. The air-flow is usually not important and so neglected and irrotational flow of incompressible water can be assumed. Because the local flow acceleration is large relative to gravitational acceleration when slamming pressure occurs, gravity acceleration is neglected. The main references are von Karman [7] and Wagner [8] methods. The first one does not consider the local rise up of the water around the hull and it proceeds to calculate the impact force through the application of the momentum theorem. The original momentum of the body is distributed at the time t between the body and the water. That part of the momentum is already transferred to the water at the time t depends on x and can be approximated as follows. With reference to Figure 2.1

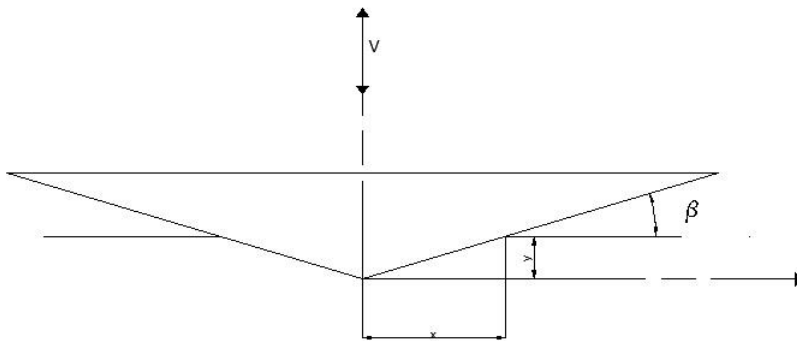


Figure 2.1: von Karman wedge

the total momentum is:

$$M = \frac{W}{g} v + \frac{1}{2} x^2 \rho \pi v \quad (2.1)$$

which must be equal to the original momentum:

$$M = \frac{W}{g} v_0 \quad (2.2)$$

v is the downward velocity, v_0 is the velocity at moment of first contact, W is the weight of the body per unit length, β is the deadrise angle and y and x are the vertical and horizontal distance through which the body travels in the time t . Setting:

$$v = \frac{dy}{dt} = tg\beta \frac{dx}{dt} \quad (2.3)$$

it is obtained

$$\frac{W}{g} \frac{dx}{dt} tg\beta \left(1 + \frac{\rho\pi gx^2}{2W} \right) = \frac{W}{g} v_0 \quad (2.4)$$

where

$$\gamma = \rho g$$

$$\frac{dx}{dt} \left(1 + \frac{\gamma\pi x^2}{2W} \right) = v_0 \cot g\beta \quad (2.5)$$

writing this in the form

$$\frac{dx}{dt} = \frac{v_0 \cot g\beta}{1 + \frac{\gamma\pi x^2}{2W}} \quad (2.6)$$

it is easy to calculate

$$\frac{d^2x}{dt^2} = \frac{d}{dx} \left[\frac{1}{2} \left(\frac{dx}{dt} \right)^2 \right] \quad (2.7)$$

finally, the expression of the impact pressure is given as:

$$P = \frac{W}{g} \frac{d^2y}{dt^2} = \frac{v_0^2 \cot g\beta}{\left(1 + \frac{\gamma\pi x^2}{2W} \right)^3} \rho\pi x \quad (2.8)$$

and the average pressure as

$$p = \frac{P}{2x} = \frac{\rho v_0^2}{2} \frac{\pi \cot g\beta}{\left(1 + \frac{\gamma\pi x^2}{2W} \right)^3} \quad (2.9)$$

the pressure is evidently maximum in the middle of the float at the moment of first contact, therefore

$$p_{max} = \frac{\rho v_0^2}{2} \pi c \cot g \beta \quad (2.10)$$

Instead, the Wagner's method take into account the rise-up of the water and semi-infinite wedge-cylinder idealization, as shown in the Figure 2.2

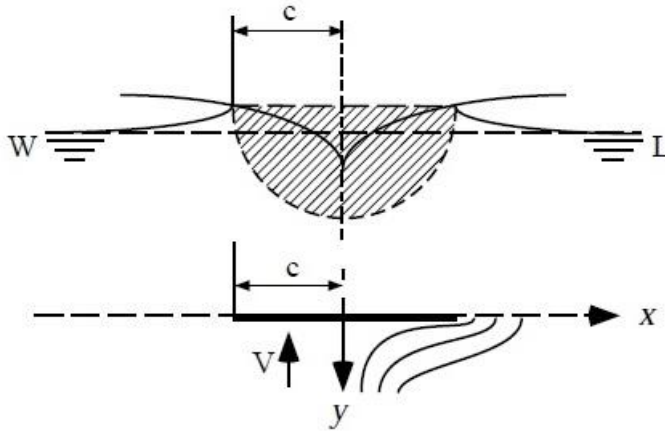


Figure 2.2: Wagner wedge

Through the Bernoulli equation:

$$\begin{aligned} \frac{p(x)}{\rho} &= \frac{\partial \phi}{\partial t} - \frac{1}{2} (\nabla \phi)^2 = \\ &= \sqrt{c^2 - x^2} \frac{dV}{dt} + V \frac{c}{\sqrt{c^2 - x^2}} \frac{dc}{dt} - \frac{1}{2} \frac{V^2 x^2}{c^2 - x^2} \end{aligned} \quad (2.11)$$

where ϕ is the velocity potential with the following boundary conditions:

$$\phi = \begin{cases} V \sqrt{c^2 - x^2} & \text{if } x < c \\ 0 & \text{if } x > c \end{cases} \quad (2.12)$$

$$\frac{\partial \phi}{\partial y} = \begin{cases} 0 & \text{if } x < c \\ \frac{V}{\sqrt{1 - \frac{c^2}{x^2}}} & \text{if } x > c \end{cases} \quad (2.13)$$

for a simple triangular wedge, with deadrise angle β , the expanding velocity of plate is

$$\frac{dc}{dt} = \frac{1}{2}\pi V \cot \beta \quad (2.14)$$

Wagner's theory gives the impact pressure as:

$$p(x) = \frac{1}{2}\rho V^2 \left[\frac{\pi \cot \beta}{\sqrt{1 - \frac{x^2}{c^2}}} - \frac{\frac{x^2}{c^2}}{1 - \frac{x^2}{c^2}} + \frac{2V}{V^2} \sqrt{c^2 - x^2} \right] \quad (2.15)$$

Zhao et al. [10] presented a generalized Wagner theory that is a simplification of the more exact solution of the water entry problem by Zhao and Faltinsen. The generalized Wagner method is more numerically robust and faster than the original exact solution. It gives satisfactory results and is therefore preferred in engineering practice.

2.2 Experimental set-up

To assess the hydrodynamic impact pressure by Faltinsen and Zhao method, experimental seakeeping tests have been done to obtain the vertical velocity as input for the analytical procedure.

All experiments are performed in the towing tank (135m x 9m x 4.2m) of DII, University of Naples Federico II with maximum towing carriage speed of 7 m/s and a multi-flap wave maker by Edinburgh Design. The hull model is a monohedral hard chine V bottom, from Begovic and Bertorello work [39], built with clear bottom and deck in order to allow the visual inspection of the wetted surface before and after the slamming impact. From a series of seakeeping tests from Begovic et al. [40] the resonant wave frequency is identified and it has been chosen as the first test parameter. Three model velocities have been identified to cover all operating speed range.

Model is connected to carriage by the measuring instrument R47, which allows model to heave and pitch, but restrict it to surge, sway, roll and yaw. The main characteristics of the model are reported in Table 2.1

Description	Symbol	Value	
Length over all	Loa	1.9	m
Length of the monohedral part	Lab	1.5	m
Breadth	B	0.424	m
Immersion	T	0.096	m
Ship Displacement	Δ	32.66	kg
Longitudinal position of GC from stern	LCG	0.73	M
Vertical position of GC from keel	VCG	0.145	m
Deadrise angle	β	16.7	deg

Table 2.1: Model characteristics

The model is ballasted to achieve a weight of 32.66 kg and trimmed to 1.66 degree. Towing force, directed horizontal to the calm water level, is applied to the model at deck level (0.18 m from baseline) and at 0.535 m from stern. Pitch and heave are measured at R47 position; heave at CG is recalculated during data elaboration. Two accelerometers Cross Bow CXL04GP3-R-AL are mounted at model, one at CG position and another one at 1.6 m from stern. Encounter wave amplitude is measured by two ultrasonic wave gauges type Baumer UNDK 301U6103/SI4, one aligned with the R47 and one 4 meters in the front of measuring arm. The model set-up is shown in Figure 2.3



Figure 2.3: Experimental set-up

All seakeeping data are sampled at frequency of 500 Hz. For purpose of this work three test conditions are considered, reported in Table 2.2

	Wave amplitude [m]	Wave frequency [Hz]	Model speed [m/s]	Encounter Frequency [Hz]
Test #1	0.032	0.65	3.4	1.56
Test #2	0.032	0.65	4.6	1.91
Test #3	0.032	0.65	5.75	2.21

Table 2.2: Seakeeping test conditions

and the following values are measured: forward speed, heave and pitch motions, vertical accelerations in two points and encounter wave (amplitude and frequency).

2.3 Seakeeping tests and pressure evaluation

From the seakeeping tests results, i.e. from the measured heave and pitch at the centre of the gravity, the vertical motion at the bow is calculated. Time series of calculated vertical motions at 1.6 meters from stern are shown in Figures 2.4. Measured accelerations at the bow section, are shown in the Figure 2.5 for the three different model speed reported in Table 2.2.

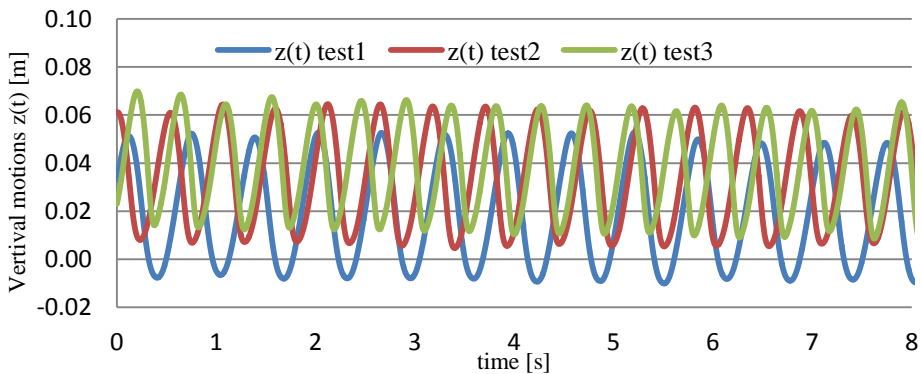


Figure 2.4: Amplitude of vertical motions at bow

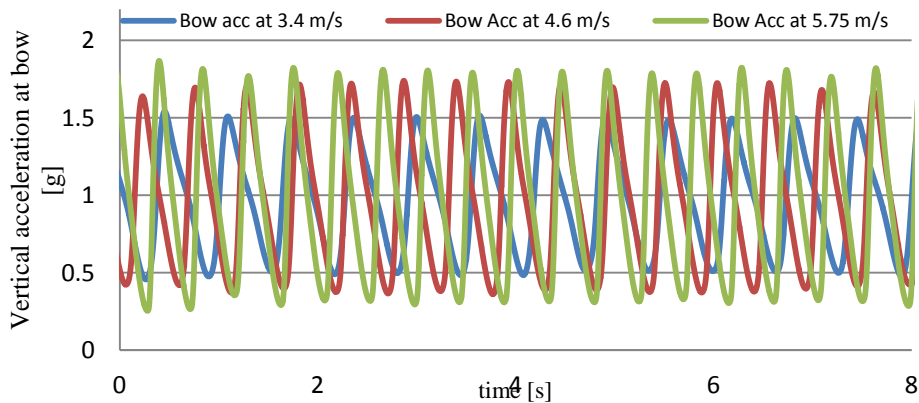


Figure 2.5: Vertical accelerations at bow

The pressure evaluation is based on the studies presented by Zhao and Faltinsen [9-11].

The following Figure 2.6, shows the predicted pressures for $20^\circ < \beta < 81^\circ$ from the Zhao and Faltinsen study [9].

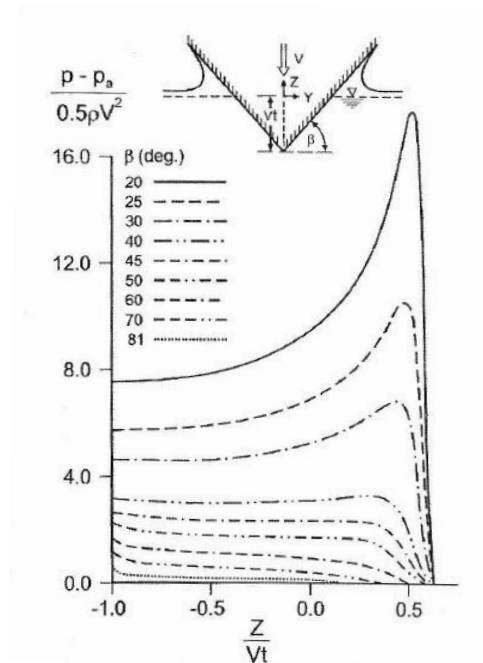


Figure 2.6: Predictions of pressure (p) distribution during water entry of a rigid wedge with constant vertical velocity V

The pressure distribution becomes pronouncedly peaked and concentrated close to the spray root when $\beta \approx 20^\circ$.

A measure of spatial extent ΔS_S of high slamming pressure is explained in Figure 2.7. The results by Zhao and Faltinsen [9] show that ΔS_S has meaning only when $\beta \leq 20^\circ$.

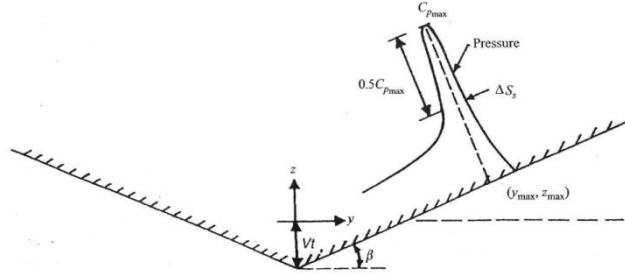


Figure 2.7: Zhao and Faltinsen diagram of hydrodynamic pressure distribution

The pressure coefficient and other parameters, defined in Figure 2.7, are reported in the following Table 2.3

$\beta [^\circ]$	C_{pmax}	z_{max}/Vt	$\Delta S_S/c$	$F_3/\rho V^3 t$
4	503.03	0.5695	0.01499	1503.638
7.5	140.587	0.5623	0.05129	399.816
10	77.847	0.5556	0.09088	213.98
15	33.271	0.5361	0.2136	85.522
20	17.774	0.5087	0.4418	42.485
25	10.691	0.4709		23.657
30	6.927	0.4243		14.139
40	3.266	0.2866		5.477

Table 2.3: Zhao and Faltinsen slamming parameters

where, β is the deadrise angle, C_{pmax} is the pressure coefficient at maximum pressure, z_{max} is the z -coordinate of maximum pressure, $c = 0.5\pi Vt$, F_3 is the vertical hydrodynamic force on the wedge and t is the time.

Thus, the parameters characterizing slamming on a rigid body with small deadrise angles are the position and the value of the maximum pressure, the time duration and the spatial extent of high slamming

pressures. A semi-empirical approach is applied to have a prediction of the hydrodynamic pressure under the hull bottom. Dimensional analysis give the relationship eq.(2.16) to evaluate the peak of pressure p :

$$p = \frac{1}{2}\rho C_p \dot{z}(t)^2 \quad (2.16)$$

ρ is the water density, $\dot{z}(t)$ is the vertical velocity and it is analysed experimentally through the seakeeping tests, C_p is the pressure coefficient which derives from Wagner theory

$$C_{pmax} = 1 + \left(\frac{\pi \cot g \beta}{2} \right)^2 \quad (2.17)$$

To obtain the $\dot{z}(t)$ value, into equation (2.16), the discrete derivative of the experimental vertical motions is made. In the following Figure 2.8, the pressure trend, for the three forward speed speeds (3.4, 4.6 and 5.75m/s, i.e. test cases 1,2,3 from Table 2.2) at the last bow's section with constant dead-rise angle is shown:

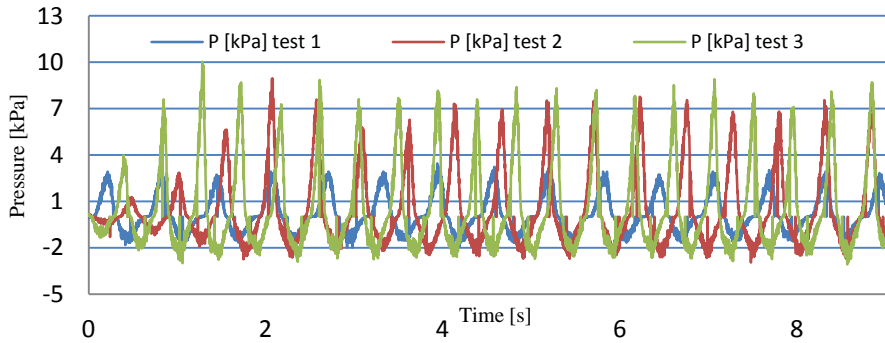


Figure 2.8: : Comparison between predicted pressure trend for three forward speed

This pressure prediction will be compared with the values of the direct measurements of the hydrodynamic and impact pressure, that is the next step of this experimental study.

The fact that the pressure distribution becomes very peaked illustrates that measurement of slamming pressure requires high sampling frequency (as shown below) and small pressure gauges.

In fact, in the most of literature references, experimental errors often depend on the size of the pressure transducers surface and on the too low sampling frequency.

3. HYDRODYNAMIC AND IMPACT PRESSURE MEASUREMENT

The major part of the experimental assessment of hydrodynamic impact pressure is performed for one impact, with the controlled vertical velocity of the wedge. In this thesis, the impact pressure has been measured for more realistic scenario, i.e. the boat operating in regular waves. In fact, analyzing a monohedral planing craft running, it is possible take into account effects like forward speed, impact with encounter waves, trim angle, air cushion under the hull bottom and other frequency components acting on the hull grider.

In this chapter the experimental campaign of the hydrodynamic pressure measurements on the hull bottom, in different regular waves, is presented.

3.1 Experimental set-up and instruments

Towing tank, acquisition system and model characteristics are the same presented for the previous seakeeping tests. Furthermore, for pressure measurements, the miniature threaded pressure sensors with stainless flush diaphragm EPX and measuring range from 0 to 1.5 bar have been adopted. In Figure 3.1, layout and dimensions of this transducer are shown:

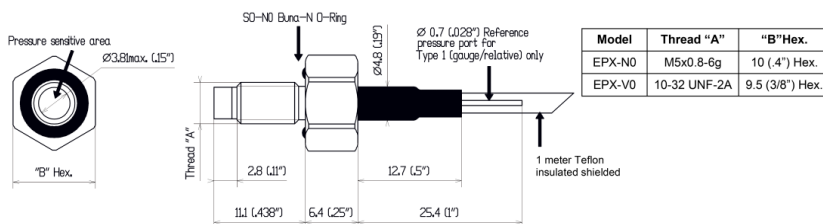


Figure 3.1: Pressure sensor model EPX-N02-1,5B-/Z2

Although the calibration certificate for any sensor is available, before doing the slamming tests, it is need to calibrate the sensors through a static test, schematically shown in Figure 3.2:

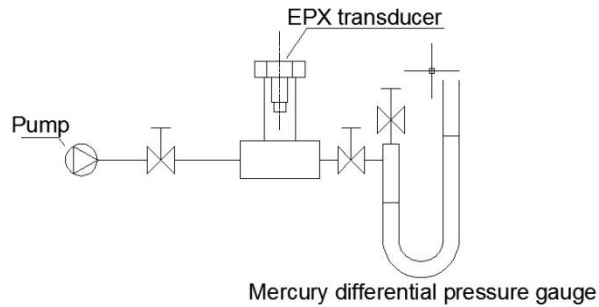


Figure 3.2: Static calibration system

in this way, the right calibration characteristic curve is created.

In the Figure 3.3, positions of the sensors, through the nine threaded holes on the plexiglass bottom are shown

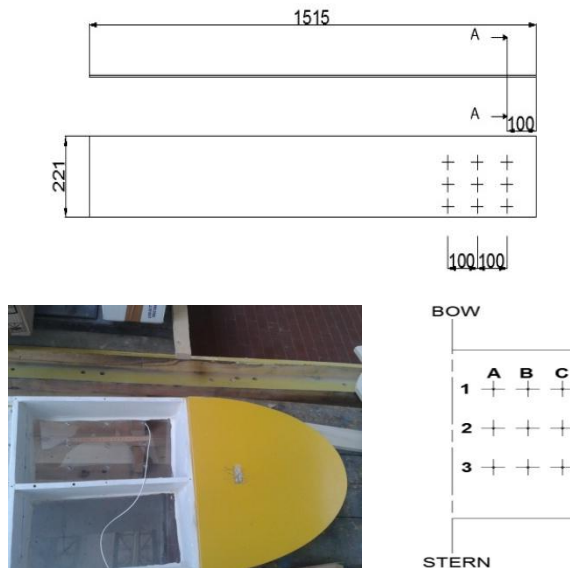


Figure 3.3: Sensor position

All the data are sampled at frequency of 5000 Hz, this choice is explained below.

In addition to the same conditions of seakeeping tests, other solutions are performed, reported in Table 3.1

	Wave amplitude	Wave frequency	Model speed	Encounter Frequency
	[m]	[Hz]	[m/s]	[Hz]
Test 1-4	0.032	0.65	3.4-4.6-5.75-6.32	1.56-1.91-2.21-2.37
Test 5-8	0.040	0.65	3.4-4.6-5.75-6.32	1.56-1.91-2.21-2.37
Test 9-12	0.028	0.65	3.4-4.6-5.75-6.32	1.56-1.91-2.21-2.37
Test 13-16	0.020	0.8	3.4-4.6-5.75-6.32	2.21-2.44-3.13-3.36
Test 17-20	0.025	0.8	3.4-4.6-5.75-6.32	2.21-2.44-3.13-3.36
Test 21-24	0.030	0.8	3.4-4.6-5.75-6.32	2.21-2.44-3.13-3.36

Table 3.1: Test conditions for pressure measurements

For the first four test conditions, the pressure in various positions, represented in Table 3.2, following the layout presented in Figure 3.3, is measured

Position name.	EPX-130KX_14	EPX-130KW_11	EPX-130KV_16
Pos1	A 1	A 2	A 3
Pos2	B 1	B 2	B 3
Pos3	C 1	C 2	C 3
Pos1T	C 1	B 1	A 1
Pos2T	C 2	B 2	A 2
Pos3T	C 3	B 3	A 3
Pos1D	C 3	B 2	A 1
Pos2D	A 3	B 2	C 1

Table 3.2: Pressure sensors positions

3.2 Experimental tests results and analysis

3.2.1 Pressure values

All the pressure time history, in the investigated positions, are reported in Appendix A.

The following Figure 3.4 shows the time histories measured during the test case 4: encounter wave amplitude, heave, pitch, bow's vertical accelerations (at 1.6 meters from stern) and the hydrodynamic pressure under the hull bottom.

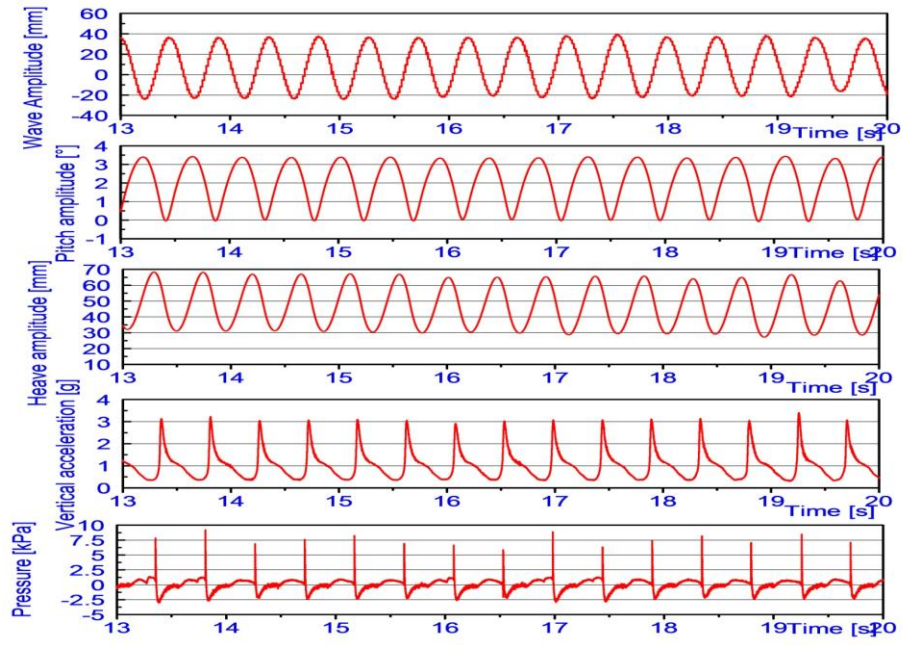
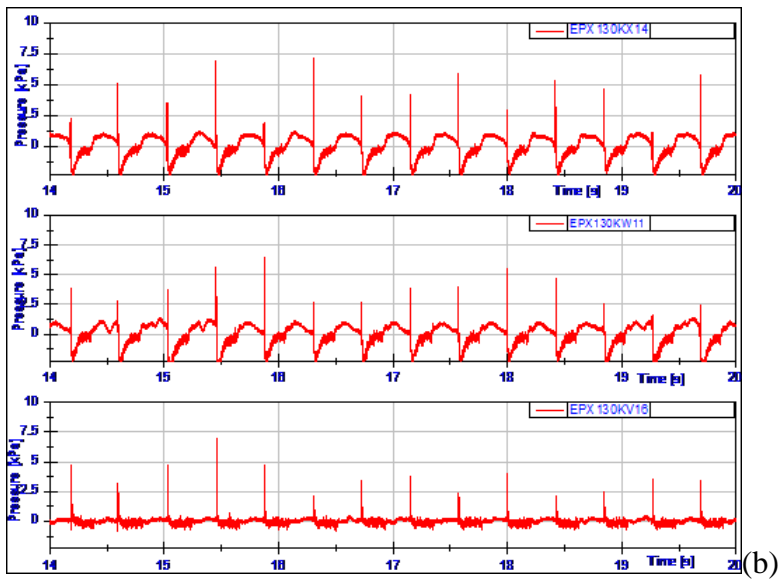
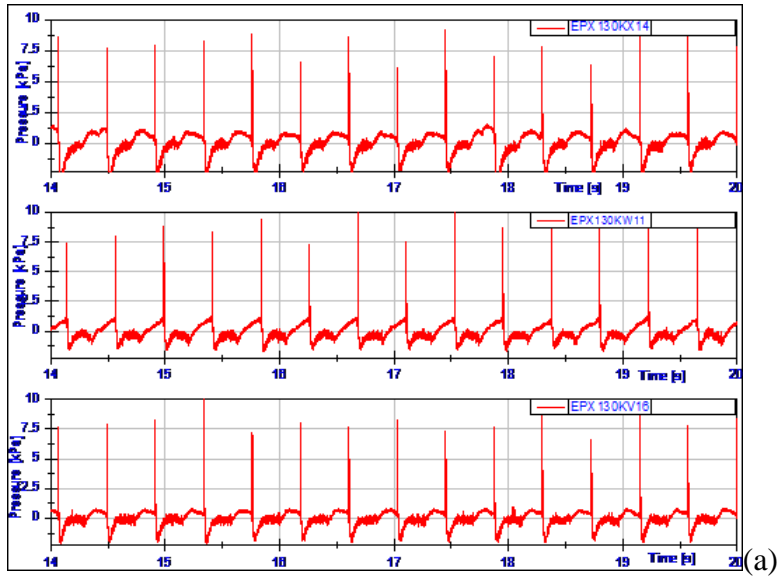


Figure 3.4: Main measured values during a run at forward speed of 6.32 m/s

An example of the pressure trend in the time domain is reported in Figure 3.5, where (a), (b) and (c) represent the three sensors longitudinal positions (see Figure 3.3). In the first group (a) the longitudinal positions are identified as A1, A2 and A3.

It is possible to observe that the pressure decrease from keel to side, and also that its trend in the time domain becomes less regular and influenced by the sprays; this fact could be noted already in the most external sensors group (c), here reported, and looking at difference between Figures A1-A12 in the Appendix A..



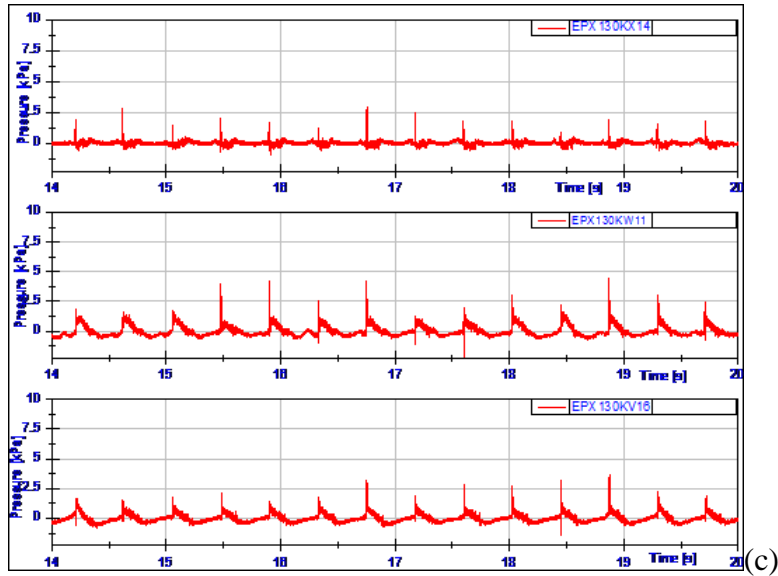


Figure 3.5: Pressure trend for positions (a) A1 A2 A3, (b) B1 B2 B3 and (c) C1 C2 C3 at model speed 6.32 m/s

Obtained pressure data has been analysed in time domain reporting the mean values of pressure peaks (p_{mean}) and also 1/3rd and 1/10th of the highest ($p_{1/3}$, $p_{1/10}$). In order to illustrate the variation of the values p_{mean} , $p_{1/3}$ and $p_{1/10}$ in function of forward speed, they are represented in Figures 3.6-3.8. It should be noted that the 1/3rd and 1/10th of highest values here do not have the same meaning as in irregular waves. As the experiments are performed in regular waves, they should be equal, but as the measurement of such an impulsive phenomenon presents intrinsic difficulties they are all reported with an idea to control data elaboration.

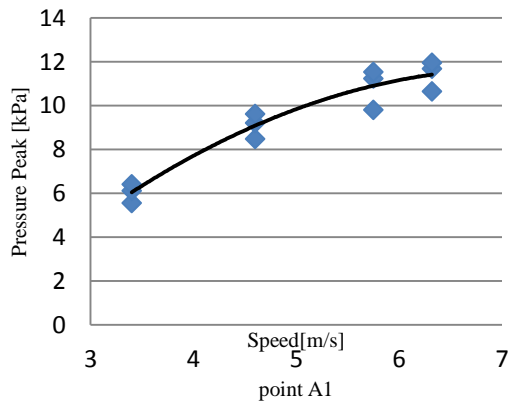


Figure 3.6: Characteristic values $p_{1/3}$, $p_{1/10}$ and p_{mean} of the pressure peaks, at point A1, in function of forward speed

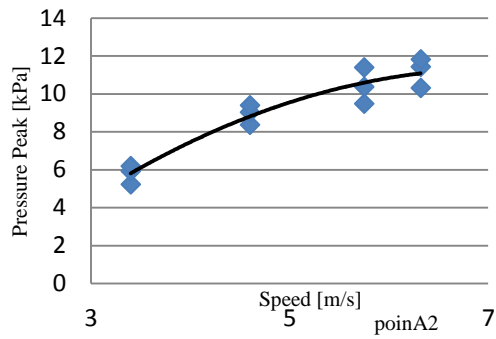


Figure 3.7: Characteristic values $p_{1/3}$, $p_{1/10}$ and p_{mean} of the pressure peaks, at point A2, in function of forward speed

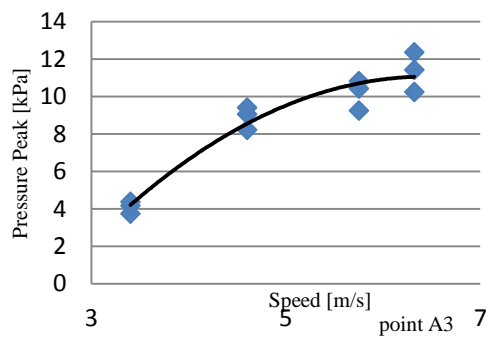


Figure 3.8: Characteristic values $p_{1/3}$, $p_{1/10}$ and p_{mean} of the pressure peaks, at point A3, in function of forward speed

Mean pressure values (p_{mean}) in all points at all model speeds represent the pressure field on the bottom panel, and is reported in Figures 3.9 and 3.10.

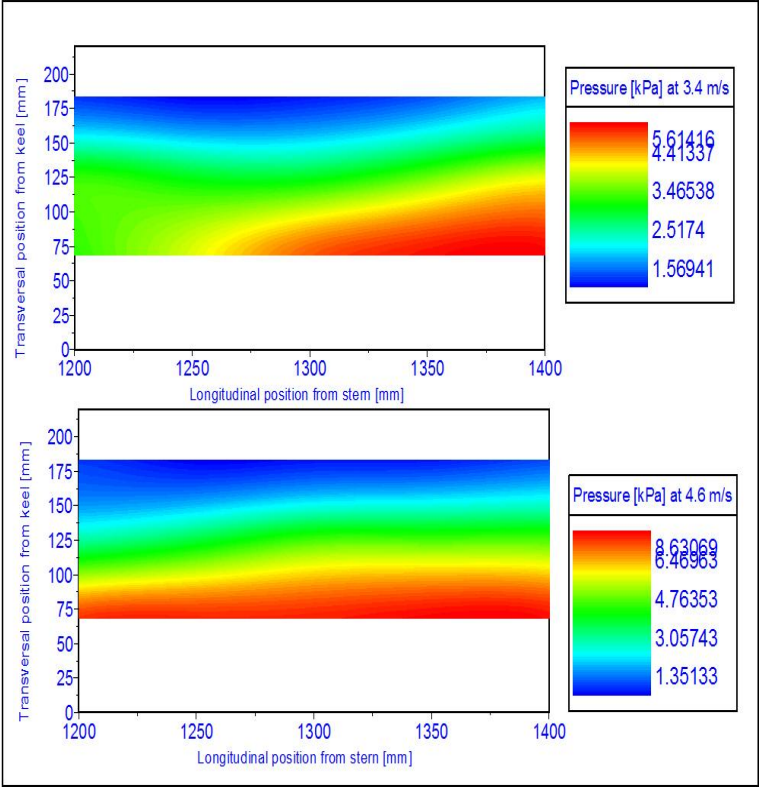


Figure 3.9: Pressure field at $v= 3.4$ and 4.6 m/s

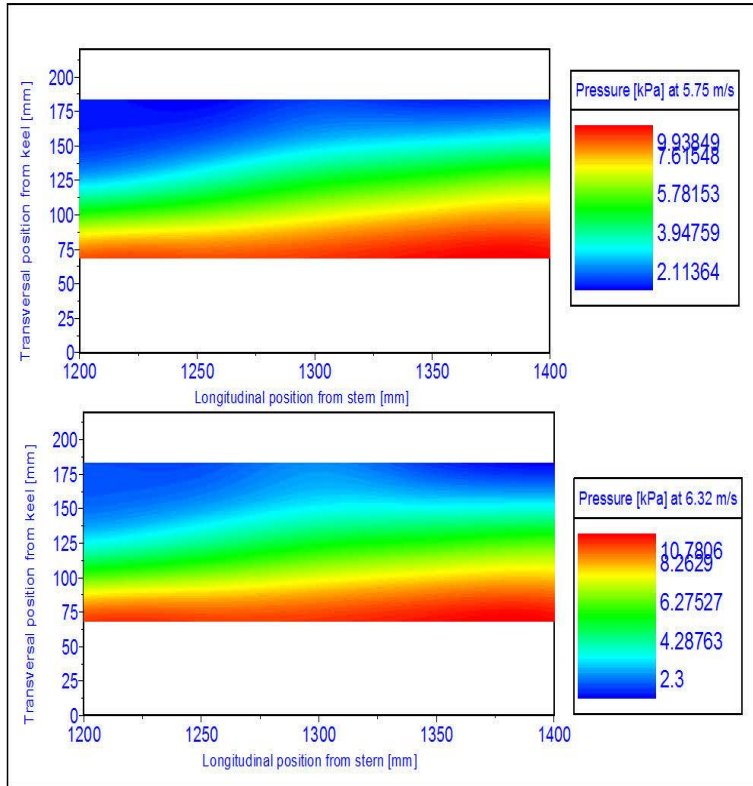


Figure 3.10: Pressure field at $v = 5.57$ and 6.32 m/s

Commenting on results shown in Figures 3.9 and 3.10, it is possible to observe that the value of the pressure peaks decreases along hull length, from bow to stern. This trend is more evident on the positions near to keel, because the measure of pressure near to side is influenced by spray.

Other tests, with different wave conditions (Tests 5 – 24 in Table 3.1), have been performed and the pressure sensors have been placed only on the three positions near to the keel (A1, A2, A3 of Figure 3.3). This solution, of sensors layout, has been adopted with the aim to observe the variation of pressure peaks with the waves frequency and amplitude, reducing the number of runs. Looking at the time history of pressure (Figures A.13 - A.31), it is possible to notice that the mean or

characteristic value of pressure peaks have a small increase with the increasing wave amplitude.

In the following Figures 3.11 and 3.12 the dimensionless mean pressure peak values ($p_{\text{mean}}/\rho g H_w$), are reported as a function of encounter wave frequency. In Figure 3.11, the dimensionless impact pressure is reported for only one encounter wave amplitude, for all three longitudinal positions nearest to keel, while in Figure 3.12 the impact pressure is made dimensionless with three different encounter wave height for position A1 only.

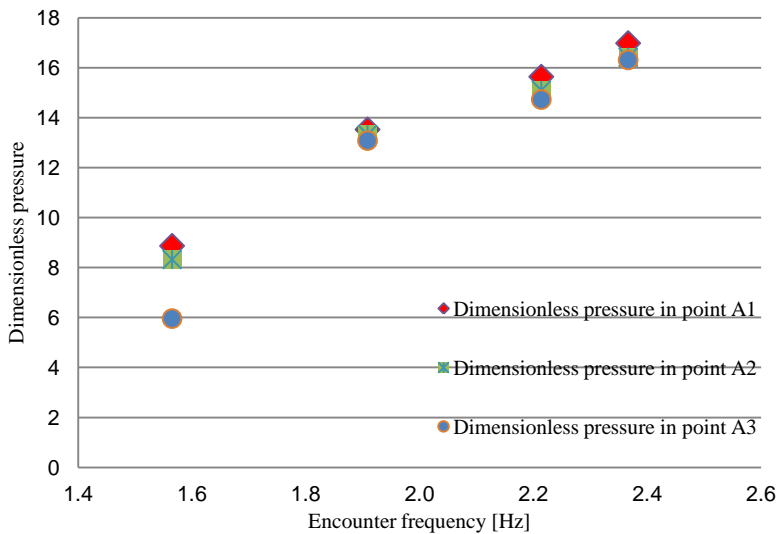


Figure 3.11: Impact pressure mean values for the longitudinal position A1, A2 and A3

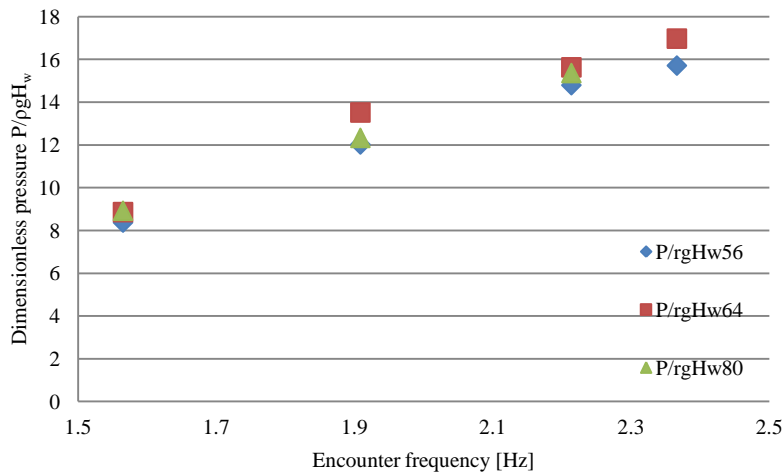


Figure 3.12: Impact pressure mean values in point A1

These diagrams shows the phenomenon linearity, changing position and wave amplitude.

From all figures can be seen that the forward speed is the most influencing parameter. As regard the effect of wave height variation on pressure, it can be seen very small variation of pressure for different wave heights. At the lower speeds there is almost no difference for different wave height indicating linear dependence on wave amplitude. At the highest speed, the highest wave amplitude test was not possible to perform due to water on deck. Measured difference should be seen more as an experimental uncertainty than as the phenomenon trend.

In this analysis the initial and final transitory part of the signals have been neglected, in order to observe a more regular phenomenon. To neglect the lowest frequency phenomena due to initial phase of the glide, an high-pass filter with a limit frequency of 1.5 Hz has been applied. Looking at the amplitude of the experimental peaks of pressure, it is possible to see that it has a very sharp shape (Figure 3.13); in particular, the time step of increasing pressure, during the

impact, is about 0.0005 seconds, confirming that the sampling frequency of 5000 Hz has been optimum to describe the pressure peaks.

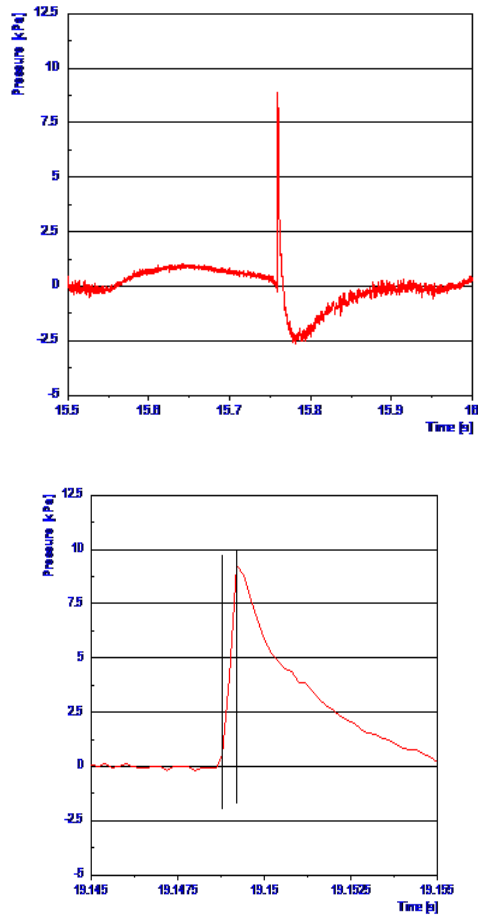


Figure 3.13: Single peak of pressure for test condition 4 at position A1

3.2.2 Analysis in the frequency domain

After the time history analysis, it is very useful, also for the next structural analysis, to study the frequency components of the measured hydrodynamic load. To transfer the pressure values from time to frequency domain (Figure 3.14) a Fourier Transform is necessary.

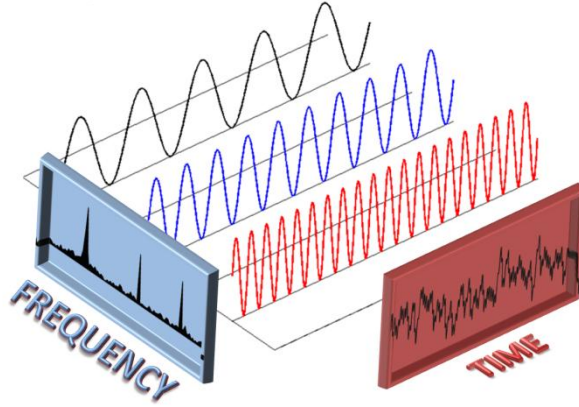


Figure 3.14: Transfer from time to frequency domain

The measured pressure can be assumed as a periodic signal $p(t)$ with period T and main frequency $F=1/T$. Every periodic signal can be represented by an infinitive series of complex coefficients (eq. 3.2) $\{P_n\}$ named Fourier Coefficient (eq.3.1), hence as a superposition of infinitive periodic signals with different main frequencies.

$$P_n = \frac{1}{T} \int_{-\frac{T}{2}}^{\frac{T}{2}} p(t) e^{-j2\pi n F t} dt \quad (3.1)$$

$$p(t) = \sum_{n=-\infty}^{\infty} P_n e^{-j2\pi n F t} \quad (3.2)$$

through this analysis it is possible to find the harmonic frequencies of the pressure signal.

The frequency response, for all points and for all forward speed, is carried out and reported in the Appendix B. The FFT of hydrodynamic pressure at point A1, A2 and A3 at model speed of 6.32 m/s is shown in the Figure 3.15. The FFT of encounter wave amplitude and vertical acceleration at bow are given in Figure 3.16.

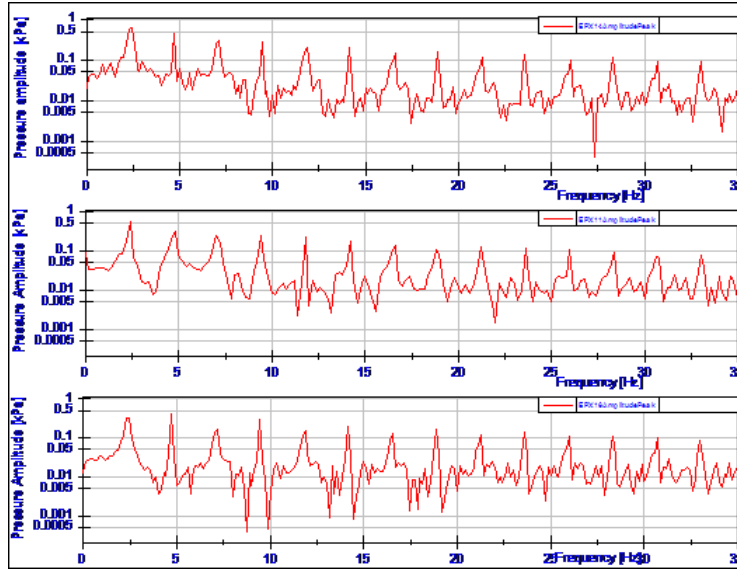


Figure 3.15: Pressure FFT for points A1, A2, A3 at model speed 6.32 m/s

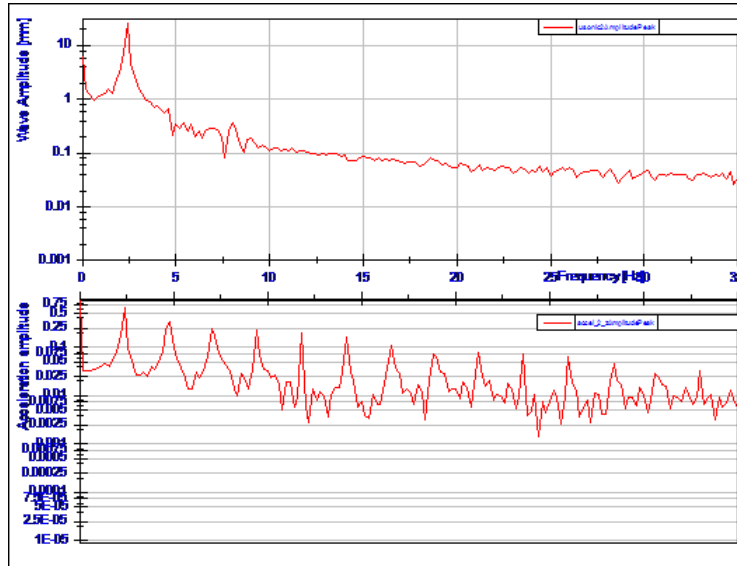


Figure 3.16: FFT of vertical acceleration and encounter wave amplitude at model speed 6.32 m/s

The frequency range of the analysis is up to 35 Hz because over this frequency the amplitude of the signals is about two order of magnitude lower than the amplitude at the main frequency. The FFT diagrams of pressure show that the phenomenon of water impact is characterized by

multiple frequencies. Note the first frequency, all the other frequencies are found to be multiple of the first (f_1). For instance, in the case of $v = 6.32$ m/s the first frequency is equal to 2.45 Hz, the second and the third ones are equal to $f_2 = 4.9$ Hz and $f_3 = 7.4$ Hz. It was seen in Begovic et al. [40] that for vertical accelerations higher order harmonics are only due to the composition of heave and pitch motions; and it is the same reason for pressure higher order harmonics. To have more information about the correlation between pressure, vertical acceleration and wave amplitude, a cross-correlation analysis is done and given in Figure 3.17.

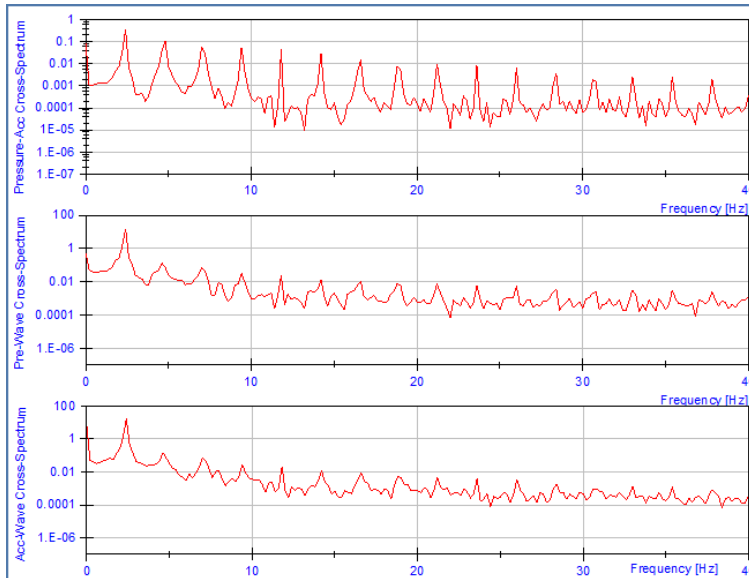


Figure 3.17: Cross-correlation analysis between pressure, acceleration and wave at point A2 at model speed of 6.32 m/s

At the first characteristic frequency (the main of the measured wave amplitude) all three signals are well correlated. In order to follow the previous analysis, for the other characteristic frequencies, only acceleration and pressure signals are well correlated, because both values depend from the vertical motions of the model.

3.2.3 Results comparison

A comparison between the measured hydrodynamic pressure and those predicted values by Faltinsen and Zhao at model speed 5.75 m/s and test case 3 (from Table 2) for point A1 is given in the Figure 3.18. It can be observed that the maximum peaks are very well predicted, the difference is about 8%

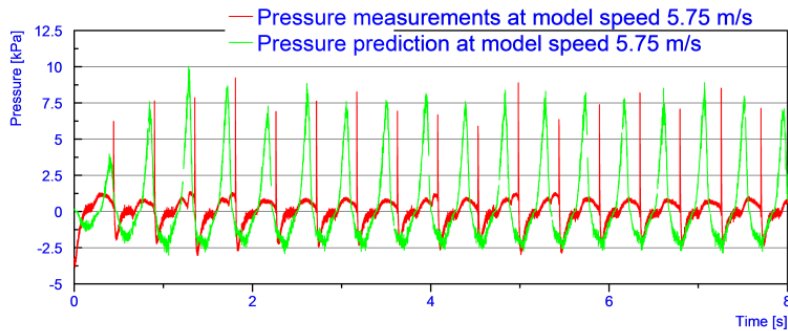


Figure 3.18: Comparison between measured and analytical hydrodynamic pressure at point A1

Further comparison with normative values of the hydrodynamic loads for planing craft (UNI EN ISO 12215) is done. In the following Table 3.3 the way to scale-down the operative conditions is shown using the methodology adopted by Lee et al [29] and Manganelli [30].

Full Scale model		Scale Factor λ	Scale model	
Ship characteristics		6.62	Model characteristics	
L_S [m]	12.58		L_M [m]	1.9
Δ_S [kg]	9460		Δ_M [kg]	32.66
V_S [kn]	31.6		V_M [m/s]	6.32
β [deg]	16.7		β [deg]	16.7
F_n	1.464		F_n	1.464
Sea conditions			Regular waves characteristics	
$H_{1/3}$ [m]	0.42		H_W [m]	0.064
Design Cat.	D		f_W [Hz]	0.65
Normative Loads			Scale Normative Loads	
$P_{BMP\ max\ S}$ [kPa]	58.7		$P_{BMP\ max\ M}$ [kPa]	8.9
$P_{BMP\ S}$ [kPa]	26.6		$P_{BMP\ M}$ [kPa]	4.0

Table 3.3: Scheme of the scale-down method

L is the length, Δ is the displacement, V is the forward speed, β the deadrise angle, Fn the Froude number, H and f are the wave height and frequency, the P_{BMP} are the normative values of hydrodynamic pressure. The subscripts S and M indicate the Ship (full scale) and Model (scale). From the $P_{\text{BMP max}}$ values in Table 3.3 it is possible to observe it is quite similar to the measured one shown in Figure 3.5 for the same conditions, with about 16% of difference.

4. PRELIMINARY INVESTIGATION ON THE DYNAMIC BEHAVIOUR OF DIFFERENT BOTTOM PANELS

After the understanding of the hydrodynamic phenomenon, and a review of the different possible methods of load assessment, the dynamic behaviour of the bottom panels, during the periodic water impact is investigated. Four different materials representative of the most used materials in the marine field, are chosen. They are glass-fiber composite, kevlar-glass fiber composite, carbon-fiber composite and light alloy 5083 .

4.1 Scantlings of full scale bottom panels

The first step of the analysis is the scantling of a real planing craft bottom panel. The considered ship is a commercial motor boat, the Gagliotta 44, shown in Figure 4.1 and 4.2.



Figure 4.1: Full-scale craft Gagliotta 44

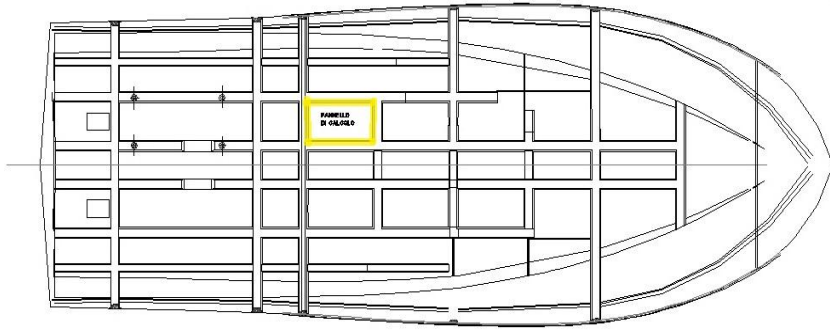


Figure 4.2: Structures plan of the full-scale craft

After the scantlings procedure, the chosen panel dimensions and characteristics are carried out and reported in Table 4.1 and 4.2 for each material

	Glass fiber composite panel	Aluminium panel	
L_P	1170	1170	mm
B_P	540	540	mm
t	11.1	8.3	mm
ψ	0.4	-	-
E	10200	70000	N/mm ²
t/w	1.64	-	mm/kg
ρ	0.0160	0.0220	g/mm ²
Weight	10.135	13.897	kg

Table 4.1: Full-scale glass fiber composite and aluminium panels characteristics

	Aramide fiber composite panel	Carbon fiber composite panel	
L_P	1170	1170	mm
B_P	540	540	mm
t	8.5	6	mm
ψ	0.5	0.55	-
E	26000	50000	N/mm ²
t/w	1.52	1.17	mm/kg
ρ	0.0120	0.0098	g/mm ²
Weight	7.556	6.203	kg

Table 4.2: Full-scale kevlar-glass fiber and carbon fiber composite panels characteristics

L_P and B_P are the panels length and breadth, t is the panels thickness, ψ is the weight percentage of fiber in the composite, E is the Young modulus, t/w is the ratio between the thickness and the mass for square meter of the fiber, and ρ is the panel density.

The hydrodynamic pressure, used for the scantling of this craft, is calculated using the ISO normative formula. This value is quite similar to the scaled-up value of the experimental maximum peak on the tested model.

4.2 Modal analysis and scantlings of the panels

In order to get further information for a better structural design of such craft, the first three mode shapes frequencies of these panels have been identified analytically and numerically.

To get an analytical guide-line, the first three natural frequencies are calculated using formulas for a rectangular plate taken from [41]. According to Blevins, it is possible to obtain the natural frequencies for different combinations of boundary conditions on the four edges of the plate, through a dimensionless frequency parameter that is a function of the boundary conditions, of the aspect ratio and, in some cases, of the Poisson's ratio of the plate.

After the analytical prediction of the natural frequencies, a numerical determination has been performed by software Nastran. The results obtained by the two methods are quite similar, with difference lower than 5%. The first three natural frequencies (f_1 , f_2 and f_3) relative to full-scale panels are reported on the following Table 4.3 and 4.4

Glass fiber composite panel		Aluminium panel	
E	10200	70000	N/mm ²
ρ	0.0160	0.0220	g/mm ²
f ₁	127.6	178.4	Hz
f ₂	158.1	221.1	Hz
f ₃	211.9	296.2	Hz

Table 4.3: Natural frequencies for full-scale glass fiber composite panel and aluminium panel

Aramide fiber composite panel		Carbon fiber composite panel	
E	26000	50000	N/mm ²
ρ	0.0120	0.0098	g/mm ²
f ₁	129.0	134.8	Hz
f ₂	159.9	167.1	Hz
f ₃	214.3	223.9	Hz

Table 4.4: Natural frequencies for full-scale kevlar-glass fiber and carbon fiber composite panels

The main dimensions, length and breadth, of the scaled-down panels are obtained with scale ratio 2, chosen for a practical construction and fitting on the panels to the model bottom. Instead, the scale panels thickness is chosen to have a similar dynamic behaviour with the full-scale panels.

The first step is to identify the dimensionless frequencies representative of both structural and hydrodynamic phenomena, two kind of relative frequencies are introduced, eq. (4.1) and eq. (4.2)

$$f_{1H}^* = \frac{f_1 H_w}{V} \quad (4.1)$$

$$f_{1t}^* = \frac{f_1 t}{V} \quad (4.2)$$

f₁ is the first natural frequency of the panel, H_w is the wave height, t is the panel thickness and V is the forward speed.

Furthermore, another dimensionless frequency, representative of the hydrodynamic phenomenon is adopted (4.3):

$$f_e^* = \frac{f_e H_W}{V} \quad (4.3)$$

f_e is the wave encounter frequency.

According to the generally used Froude theory F_n is the same for the scale model and full-scale craft. The thickness of the scale panels is chosen to achieve the most similar values of the dimensionless frequencies f_{1H}^* , f_{1t}^* and f_e^* between the scale model and the full-size craft.

After an iterative procedure, the final dimensions of the scale bottom panels have been carefully chosen, and reported in the following Table 4.5 and 4.6

	Glass fiber composite panel	Aluminium panel	
L_P	585	585	mm
B_P	270	270	mm
t	5	3.5	mm
ψ	0.4	-	-
E	10200	70000	N/mm ²
t/w	1.64	-	mm/kg
ρ	0.0076	0.00928	g/mm ²
Weight	1200	1465	g

Table 4.5: Model scale glass fiber composite and aluminium panels characteristics

	Aramide fiber composite panel	Carbon fiber composite panel	
L_P	585	585	mm
B_P	270	270	mm
t	4	2.5	mm
ψ	0.5	0.55	-
E	26000	50000	N/mm ²
t/w	1.52	1.17	mm/kg
ρ	0.0048	0.0044	g/mm ²
Weight	758	689	g

Table 4.6: Model scale kevlar-glass fiber and carbon fiber composite panels characteristics

The same modal analysis procedure is used to study the obtained scale panels.

In the following Table 4.7 and 4.8 the first three natural frequencies, relative to scale panels, are reported.

	Glass fiber composite panel	Aluminium panel	
E	10200	70000	N/mm ²
ρ	0.076	0.00928	g/mm ²
f_1	229.9	300.9	Hz
f_2	284.9	372.9	Hz
f_3	381.7	499.6	Hz

Table 4.7: Natural frequencies for scale glass fiber composite panel and aluminium panel

	Aramide fiber composite panel	Carbon fiber composite panel	
E	26000	50000	N/mm ²
ρ	0.0048	0.0044	g/mm ²
f_1	242.9	224.7	Hz
f_2	301.0	278.4	Hz
f_3	403.3	373.1	Hz

Table 4.8: Natural frequencies for scale kevlar-glass fiber and carbon fiber composite panels

And the first three modes shape of the scale panels are shown in Figure 4.3

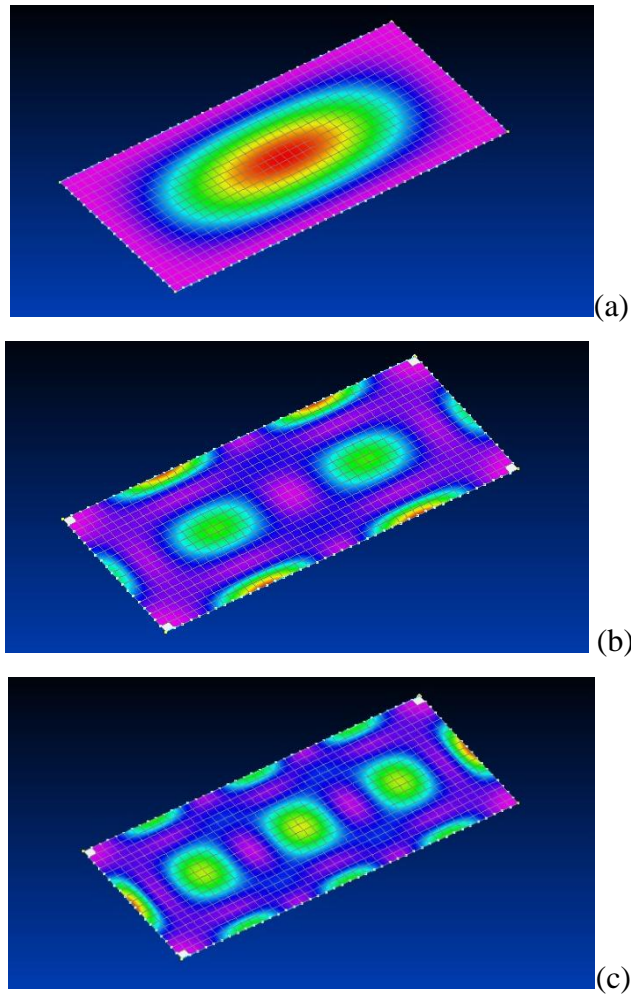


Figure 4.3: (a) mode 1, (b) mode 2 and (c) mode 3 of composite scale panels

4.3 Preliminary dynamic analysis of the panels under the hydrodynamic load

After the indentifying of the mode shapes, it is useful to analyse the dynamic behaviour applying the measured hydrodynamic load and see which panels characteristic frequencies are more excited and the maximum displacement of the panels. Through this analysis, it is

possible to have an indication about which frequencies to avoid due to machinery (engine, shaft, generators, ecc) or to hydrodynamic loads.

4.3.1 Hydrodynamic load definition

Changing the model dimensions, it is necessary to adapt also the values of forward speed and hydrodynamic pressure, following the Froude method as applied in [30]. Furthermore, the pressure values are available only for the nine measurement points (see Figure 3.3). To get the pressure distribution along all panel surface, an interpolation equation for each forward speed is proposed:

$$V = 4.1 \text{ m/s} \rightarrow p = 4.0279 + 0.0341x + 0.0057y - 0.0002x^2 - 0.0001xy \quad (4.4)$$

$$V = 5.53 \text{ m/s} \rightarrow p = 16.7804 - 0.1014x + 0.0102y + 0.0001x^2 \quad (4.5)$$

$$V = 6.91 \text{ m/s} \rightarrow p = 19.5737 - 0.151x + 0.0165y + 0.0003x^2 \quad (4.6)$$

$$V = 7.6 \text{ m/s} \rightarrow p = 20.7446 - 0.1654x + 0.0263y + 0.0003x^2 \quad (4.7)$$

In the previous equations p is the pressure value as function of x and y coordinates of the bottom panel and provides the pressure distribution in the space domain for one time instant.

To implement a dynamic analysis, the software FEMAP is adopted for the NASTRAN model pre-processing.

Imposed the geometry and mesh characteristics of the flat plate, all the four edges are set as fixed constraints; the measured hydrodynamic load is introduced as distributed with the time variation experimentally measured. The analysis is implemented for the four material characteristics, before presented, and for three different load conditions.

4.3.2 Dynamic analysis results

Some examples of the dynamic analysis results for the chosen materials panels at forward speed of 5.53 m/s is reported in Figures 4.4 - 4.7.

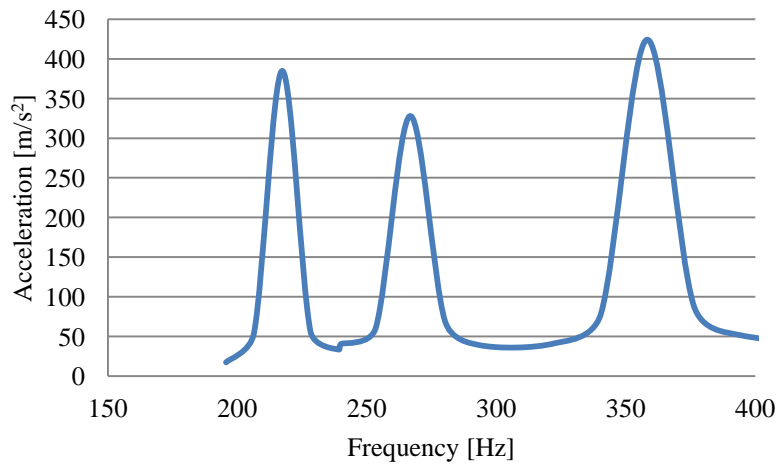


Figure 4.4: Glass fiber composite panel dynamic response at model speed of 5.53 m/s

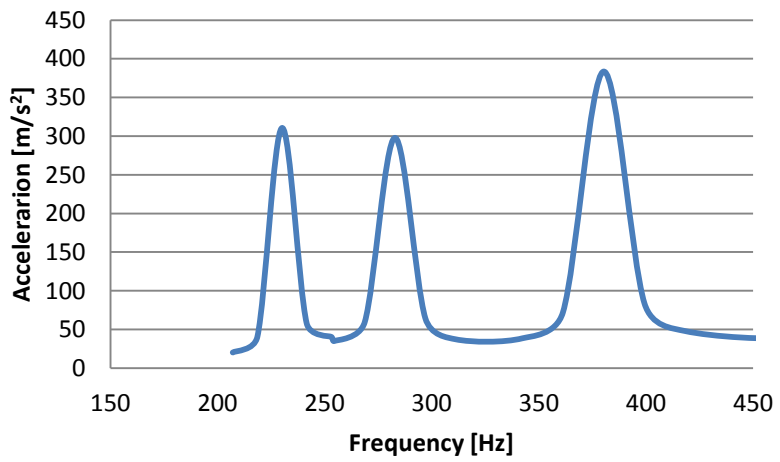


Figure 4.5: Glass-kevlar fiber composite panel dynamic response at model speed of 5.53 m/s

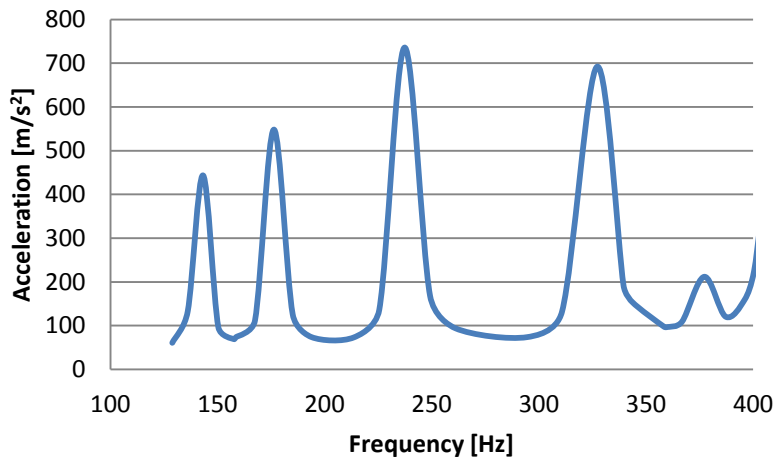


Figure 4.6: Carbon fiber composite panel dynamic response at model speed of 5.53 m/s

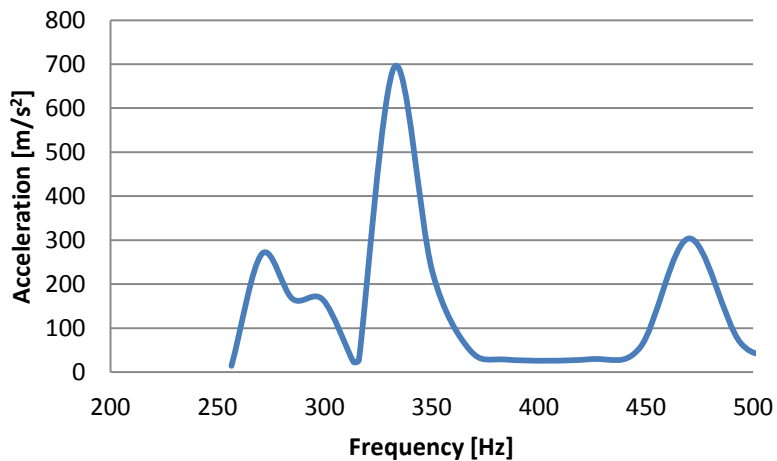


Figure 4.7: Aluminium panel dynamic response at model speed of 5.53 m/s

It is possible to observe, for the considered forward speed and for the glass fiber composite panel, that the most excited mode shape is the third one at frequency of 358 Hz, with an acceleration of 424 m/s^2 which corresponds to the maximum deflection of 3.3 mm.

This results have been carried out for all forward speed.

The next step will be the implementation of an Experimental Modal Analysis (EMA) procedure to the considered panels aimed at

determining FRF (Frequency Response Function) of each panel and a numerical-experimental correlation.

5. CONCLUSIONS

After the analytical study of the water entry of a rigid wedge through the Zhao and Faltinsen approach, following the Wagner theory, a prediction of the hydrodynamic pressure has been carried out starting from the common seakeeping tests results.

In the next step, the impact of water on a monohedral planing craft has been studied experimentally in regular waves at four model velocities measuring hydrodynamic pressure on the bottom by nine sensors and comparing them with the predicted ones.

Analysis of measured data identified multiple frequencies responses of pressure and accelerations due to the motions combination. In the considered range of wave heights, the pressure behaviour is found almost linear. At all tested velocities the maximum pressure field has been close to the keel, and decreases moving offset from the centreline. The pressure reaches its maximum value at the forward position and decreases going aft.

After the results analysis, a correlation between model and real craft has been done with the aim to have also a comparison with the normative values of the pressure.

As a further contribution to the structural design procedure a description of the dynamic behaviour of the bottom panels made by four different materials has been analysed in ship and model scale by NASTRAN software reporting first three natural frequencies and the dynamic response under the hydrodynamic load action. Particular attention has been paid to define the dimensionless frequencies which will describe scaling effect properly.

The next steps of this study will be the Experimental Modal Analysis (EMA) of the panels in model scale, after assembling to the hull bottom

in dry condition, and the Operational Modal Analysis (OMA) during the towing tests in the towing tank. The scheduled experimental campaign is aimed at verifying the representation of the phenomenon in model scale and at observing the eventual hydro-elastic coupling effects, through the comparison of the Frequency Response Functions.

APPENDIX A

PART I

In this part of appendix, the diagrams of the pressure trend for every test speeds and for all points, are shown. The position of the pressure sensors, on the flat panel of bottom, is described in Figure 3.3 and Table 3.2.

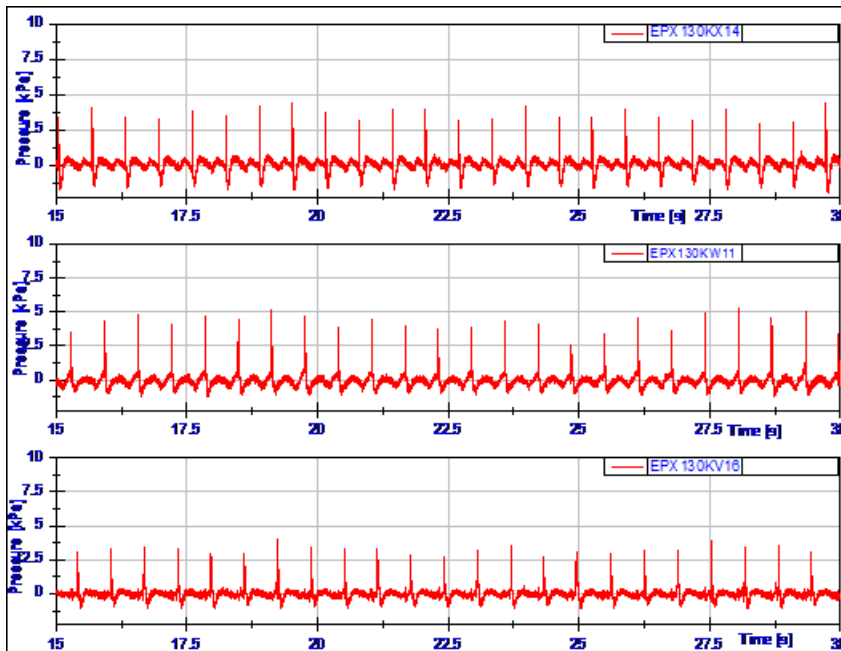


Figure A1: Pressure trend for position Pos1 at model speed 3.4 m/s

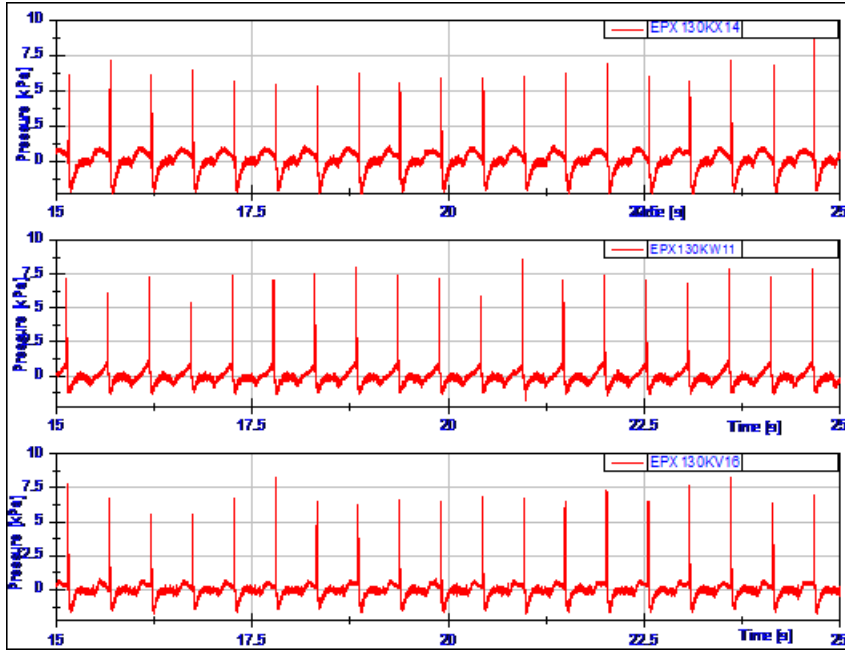


Figure A.2: Pressure trend for position Pos1 at model speed 4.6 m/s

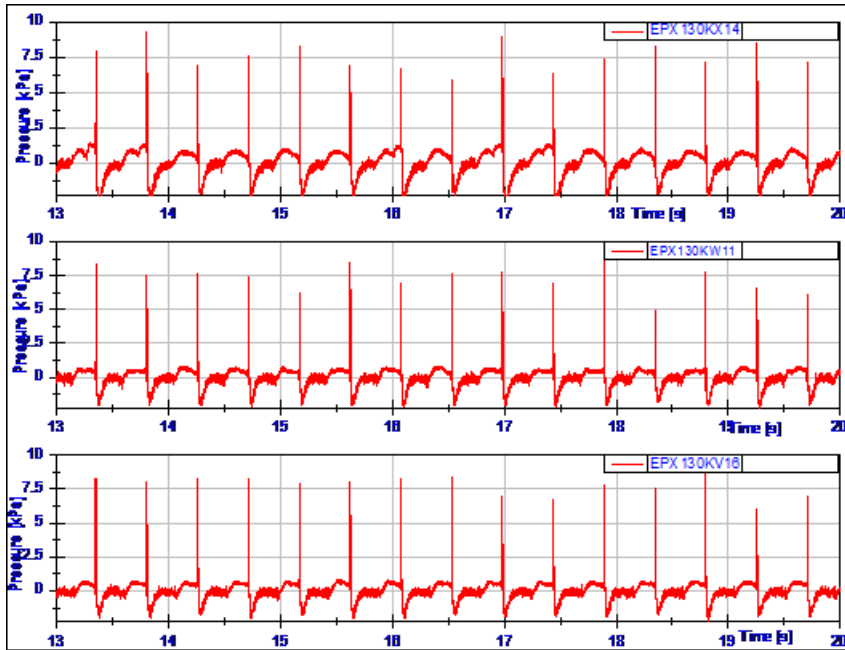


Figure A.3: Pressure trend for position Pos1 at model speed 5.75 m/s

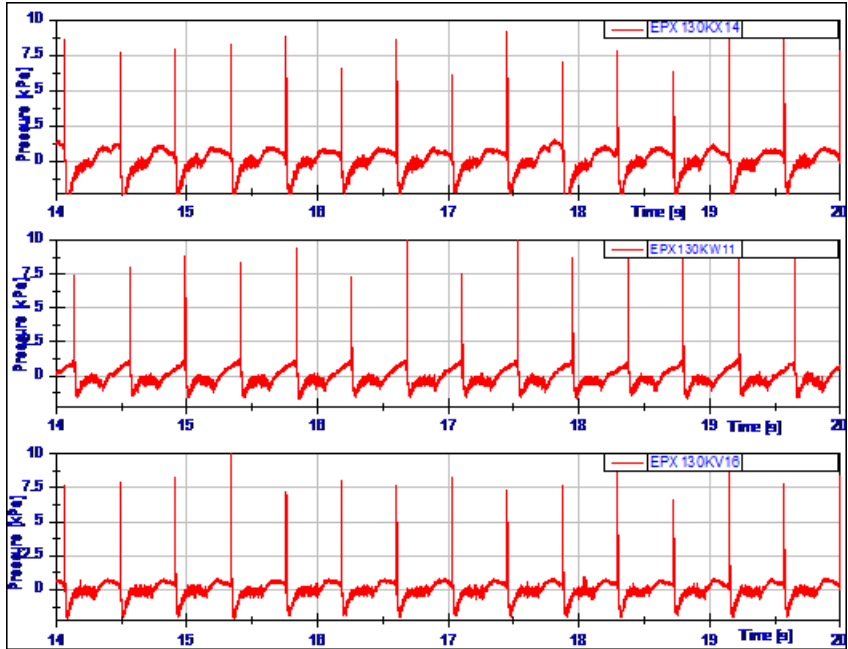


Figure A.4: Pressure trend for position Pos1 at model speed 6.32 m/s

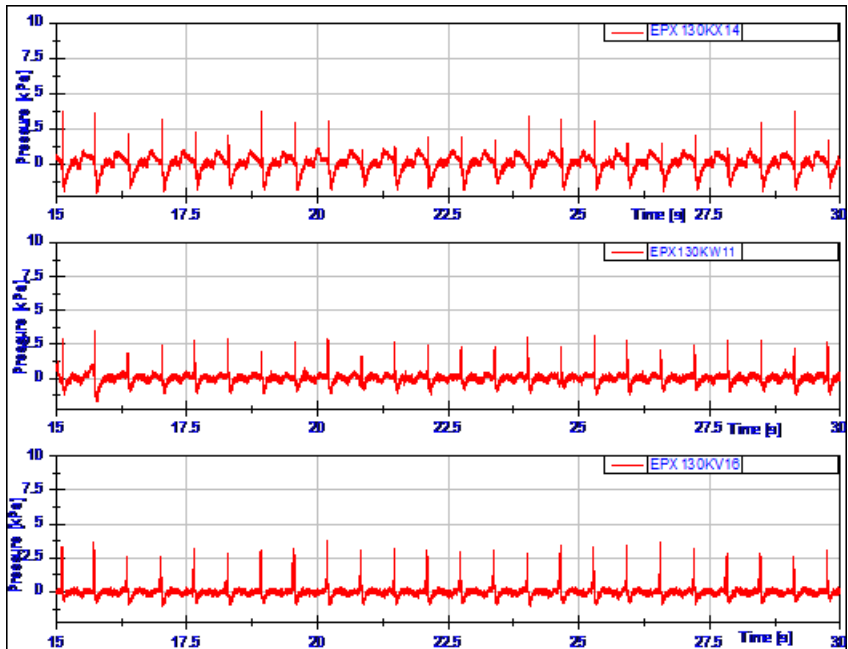


Figure A.5: Pressure trend for position Pos2 at model speed 3.4 m/s

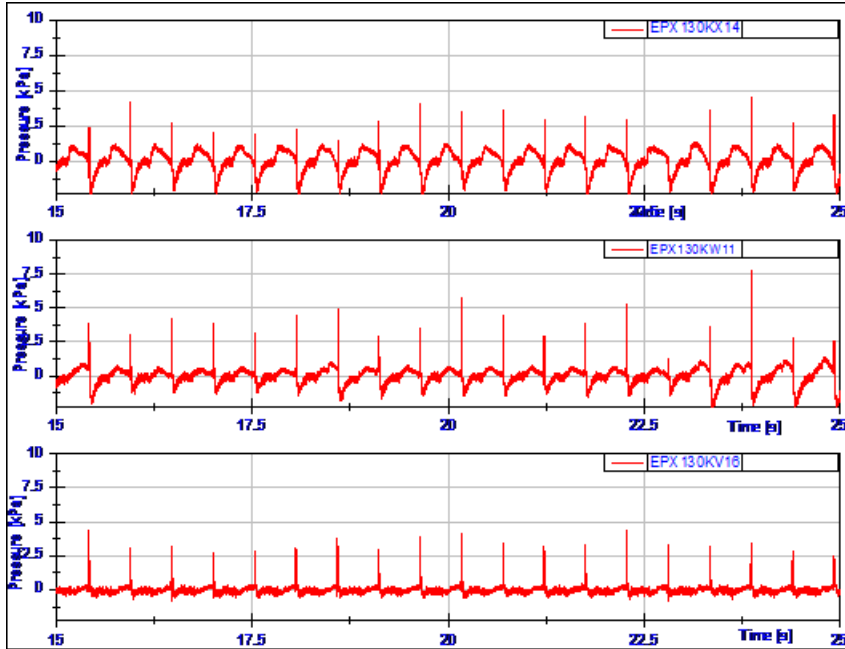


Figure A.6: Pressure trend for position Pos2 at model speed 4.6 m/s

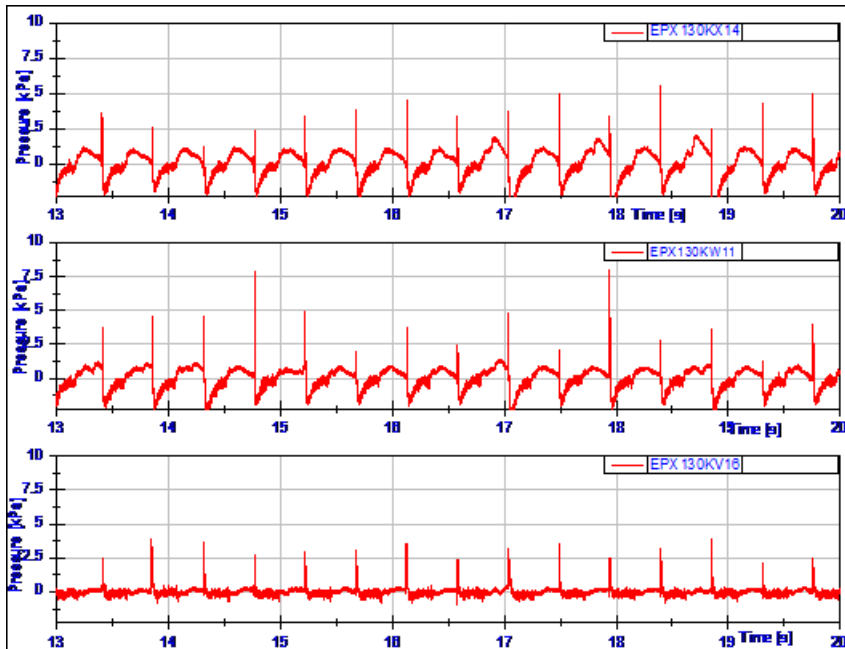


Figure A.7: Pressure trend for position Pos2 at model speed 5.75 m/s

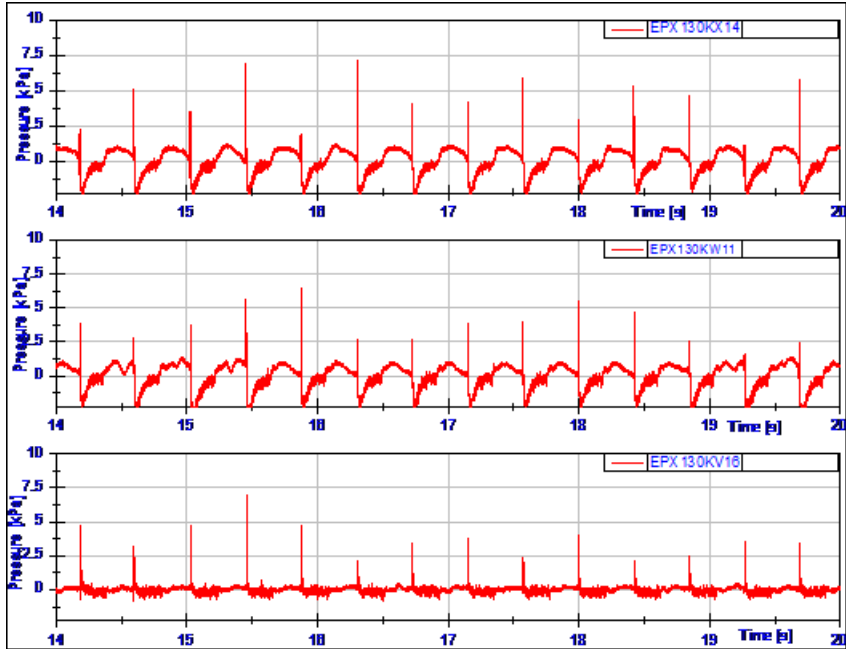


Figure A.8: Pressure trend for position Pos2 at model speed 6.32 m/s

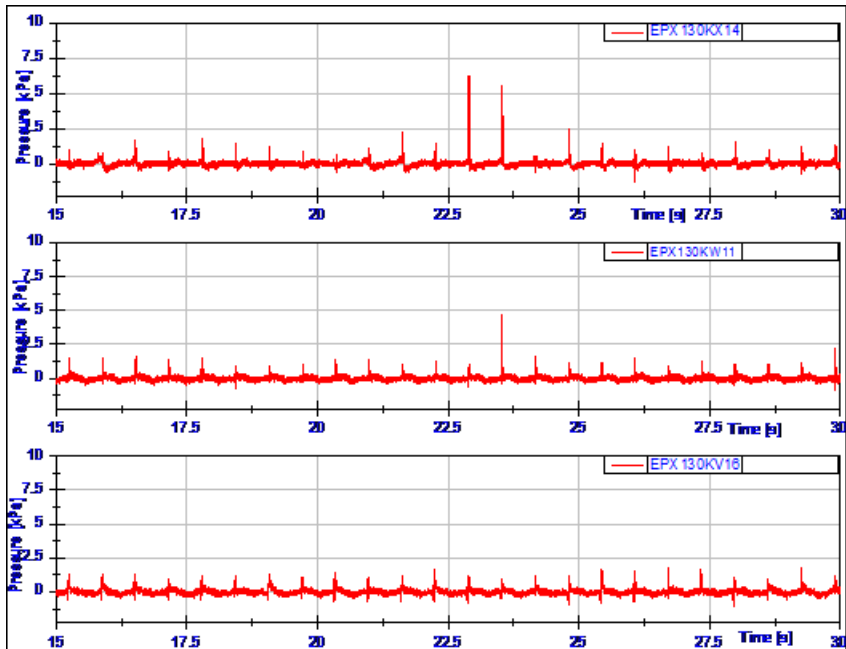


Figure A.9: Pressure trend for position Pos3 at model speed 3.4 m/s

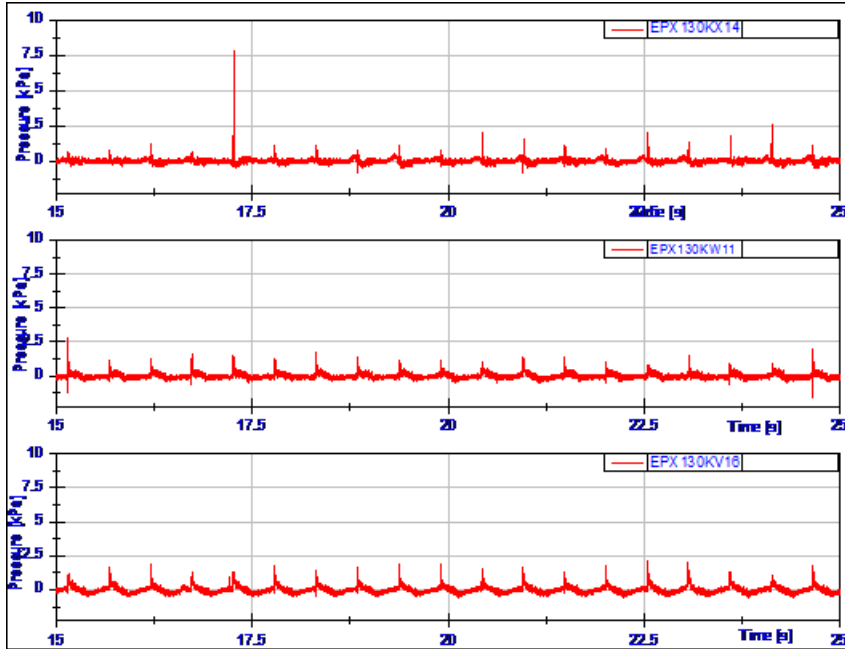


Figure A.10: Pressure trend for position Pos3 at model speed 4.6 m/s

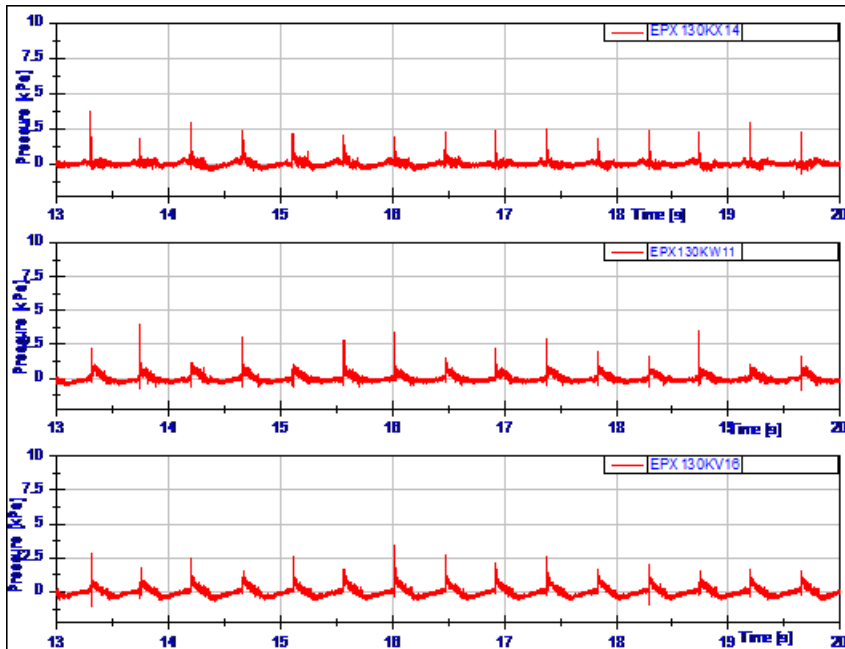


Figure A.11: Pressure trend for position Pos3 at model speed 5.75 m/s

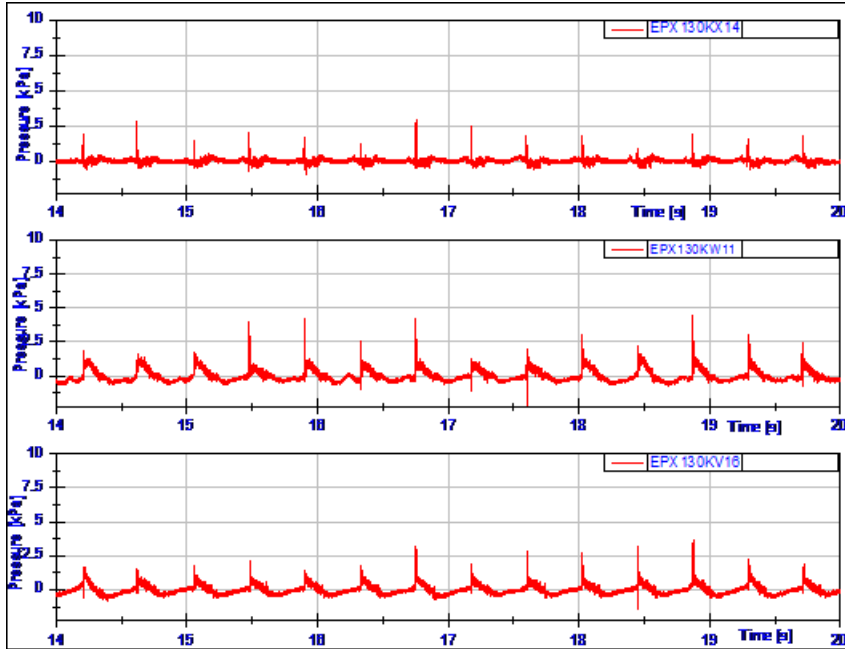


Figure A.12: Pressure trend for position Pos3 at model speed 6.32 m/s

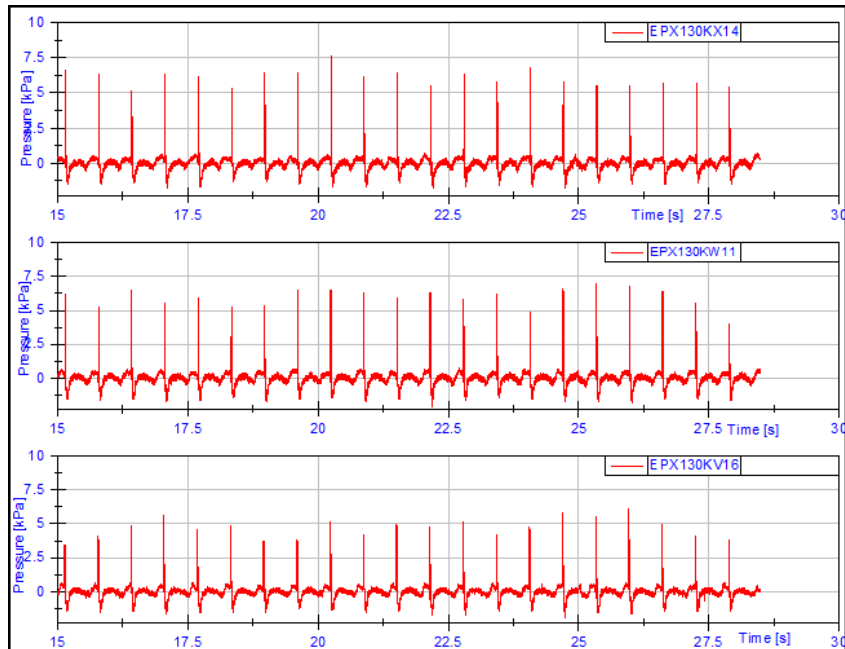


Figure A.13: Pressure trend for position Pos1 at Test 5

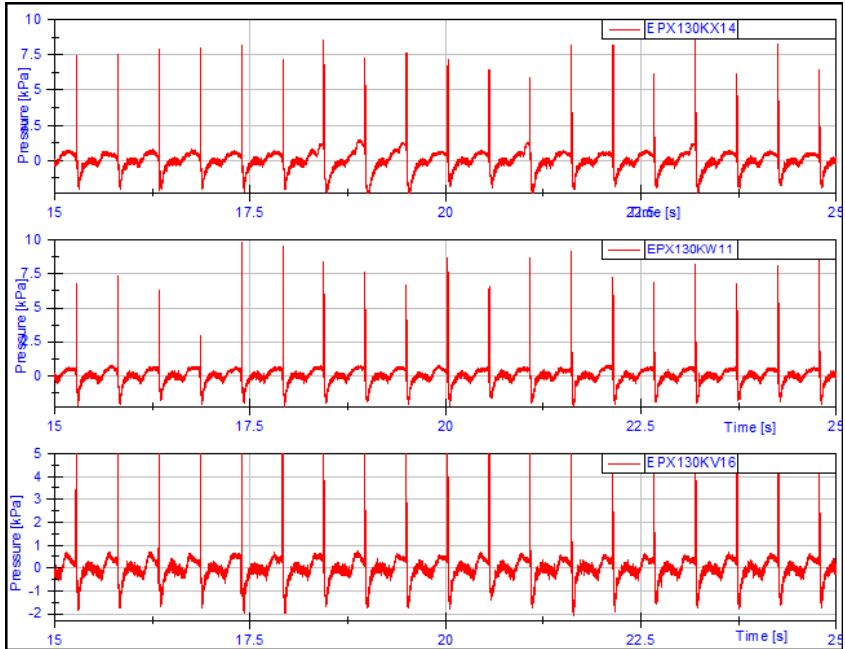


Figure A.14: Pressure trend for position Pos1 at Test 6

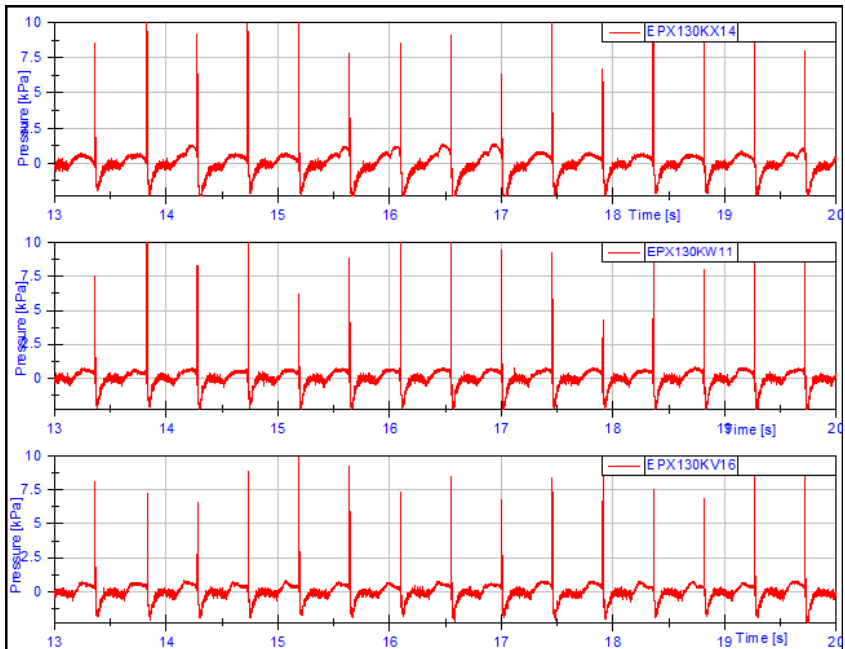


Figure A.15: Pressure trend for position Pos1 at Test 7

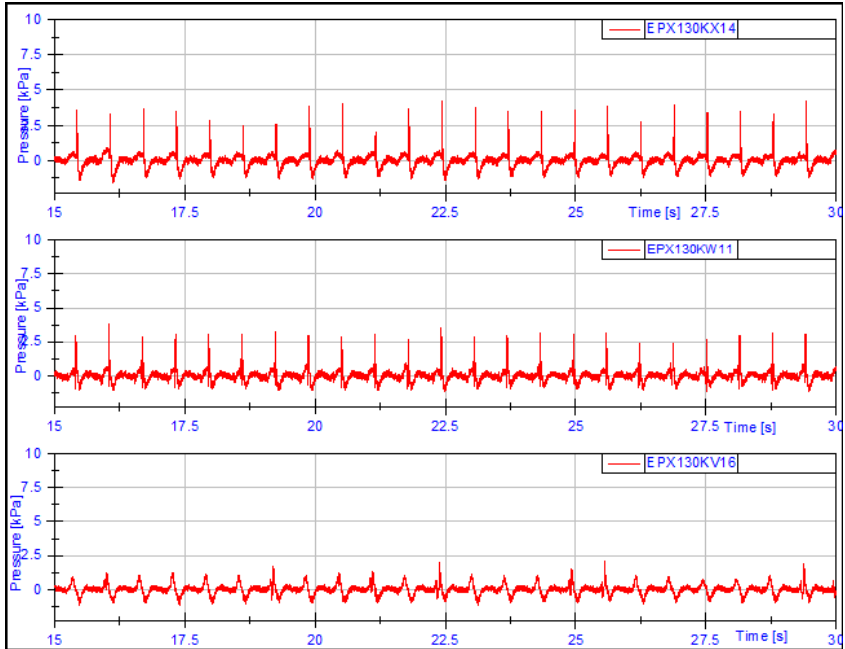


Figure A.16: Pressure trend for position Pos1 at Test 9

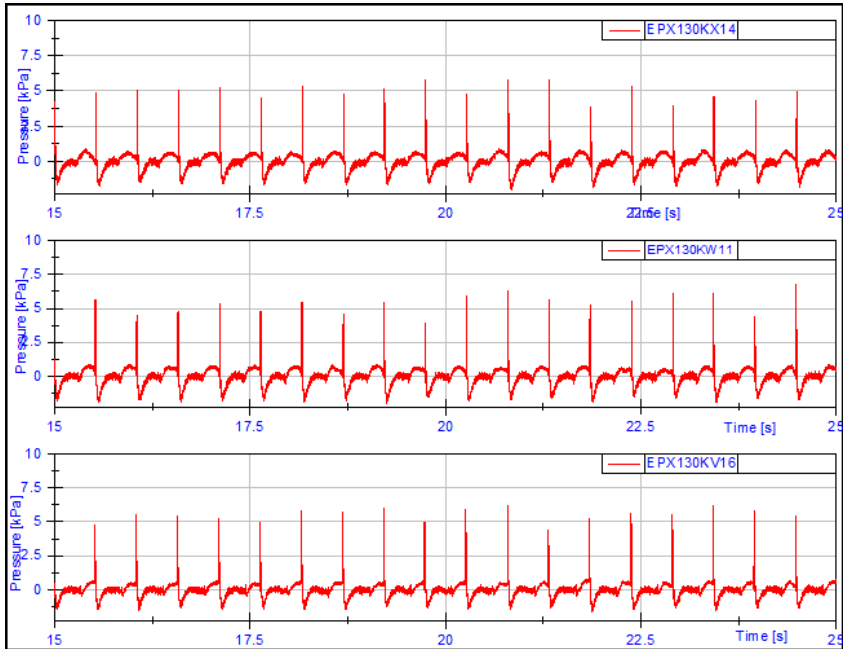


Figure A.17: Pressure trend for position Pos1 at Test 10

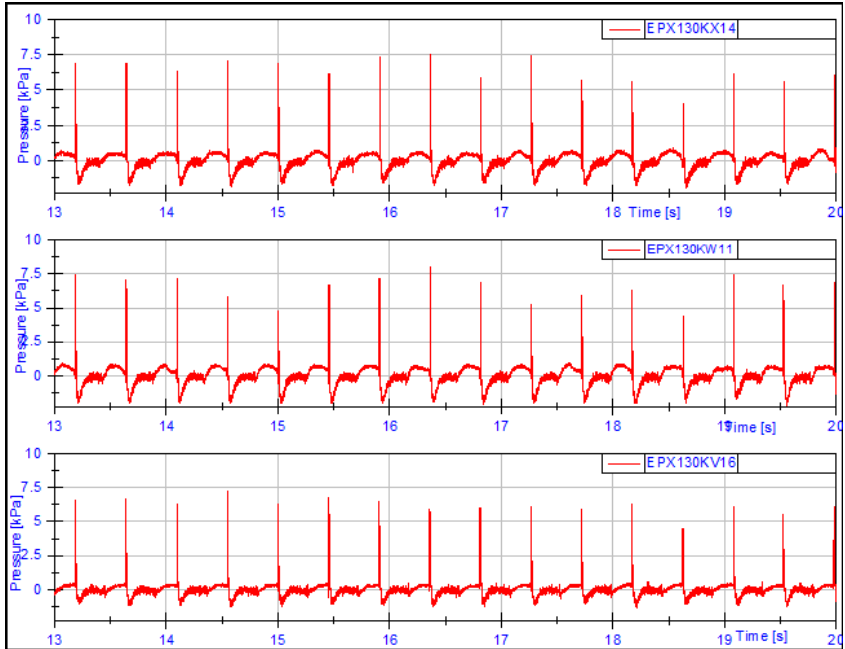


Figure A.18: Pressure trend for position Pos1 at Test 11

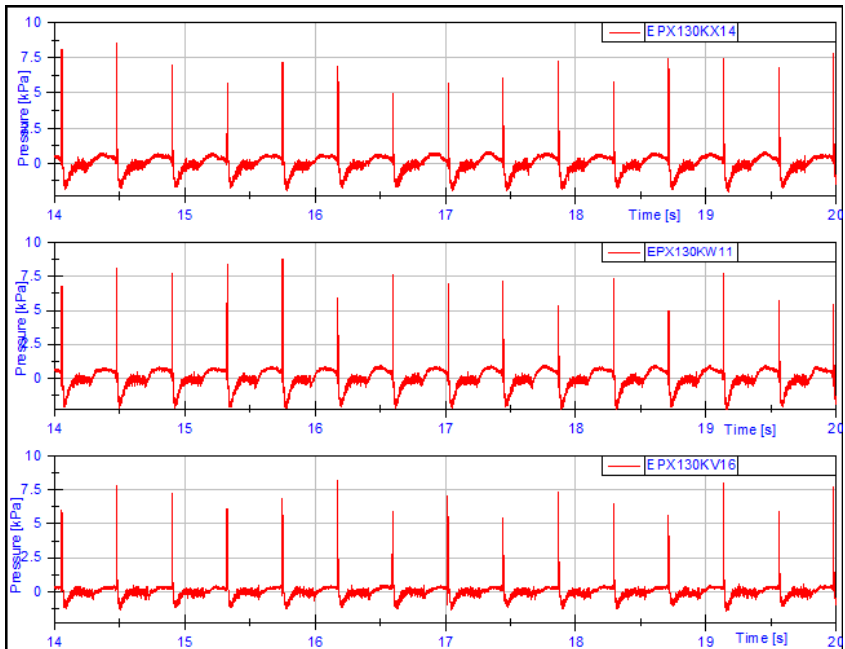


Figure A.19: Pressure trend for position Pos1 at Test 12

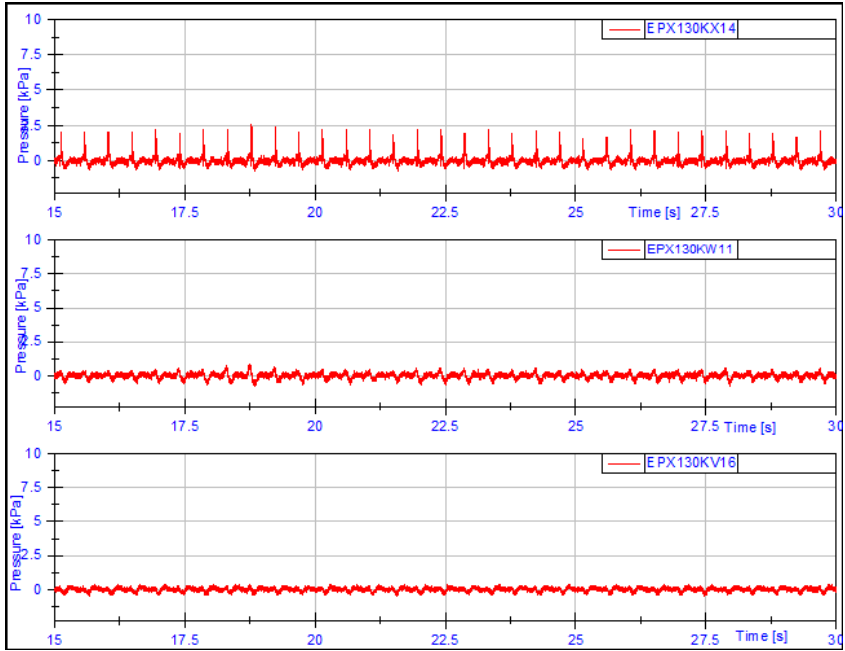


Figure A.20: Pressure trend for position Pos1 at Test 13

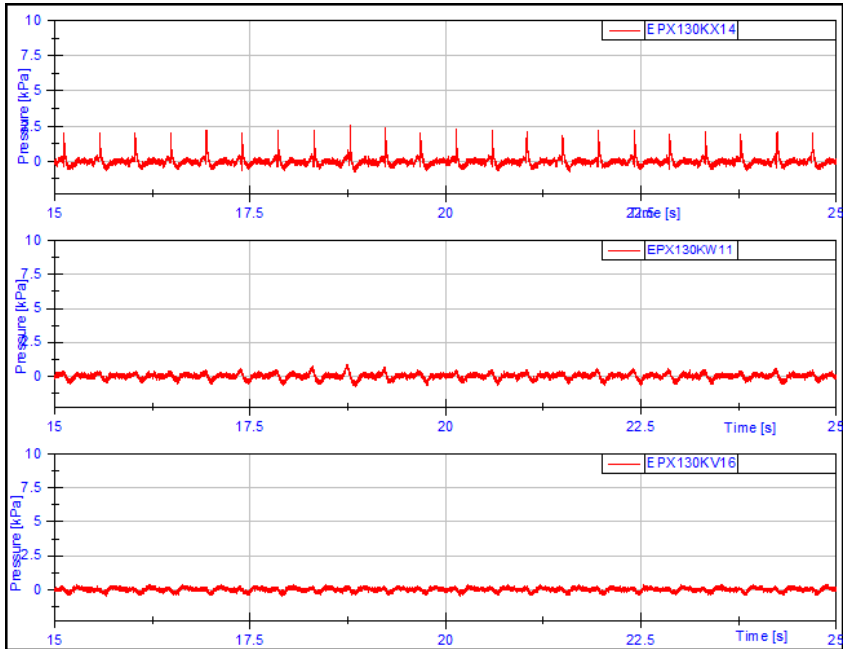


Figure A.21: Pressure trend for position Pos1 at Test 14

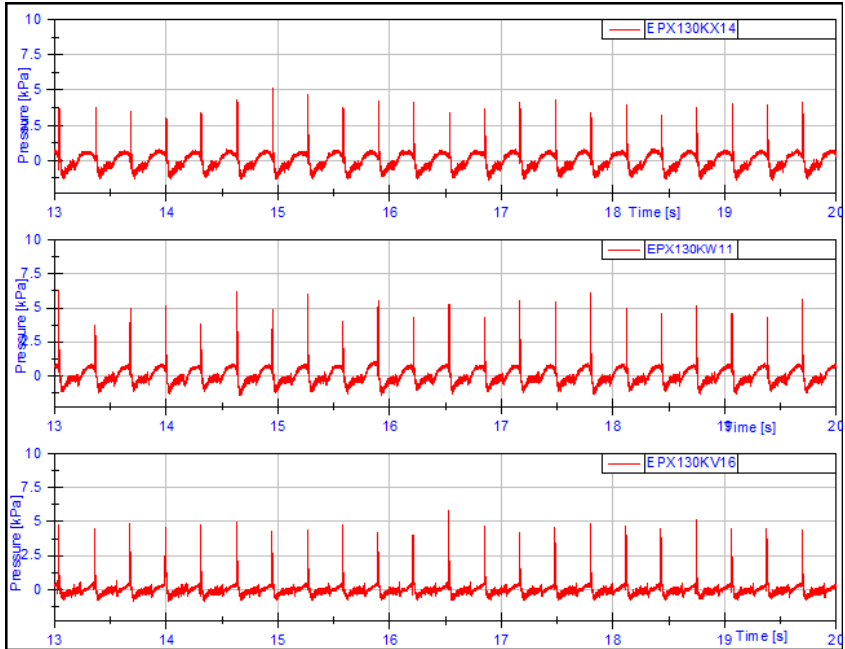


Figure A.22: Pressure trend for position Pos1 at Test 15

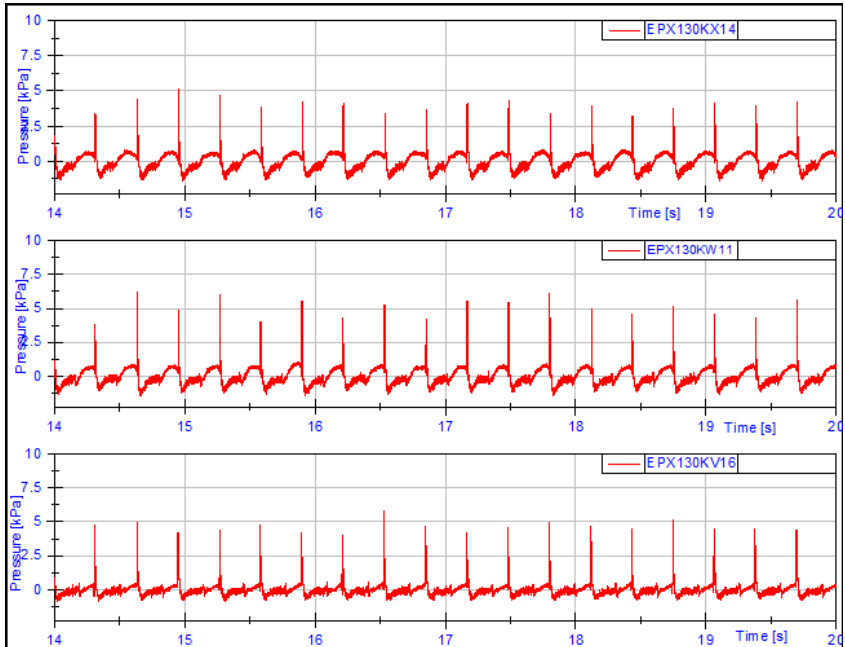


Figure A.23: Pressure trend for position Pos1 at Test 16

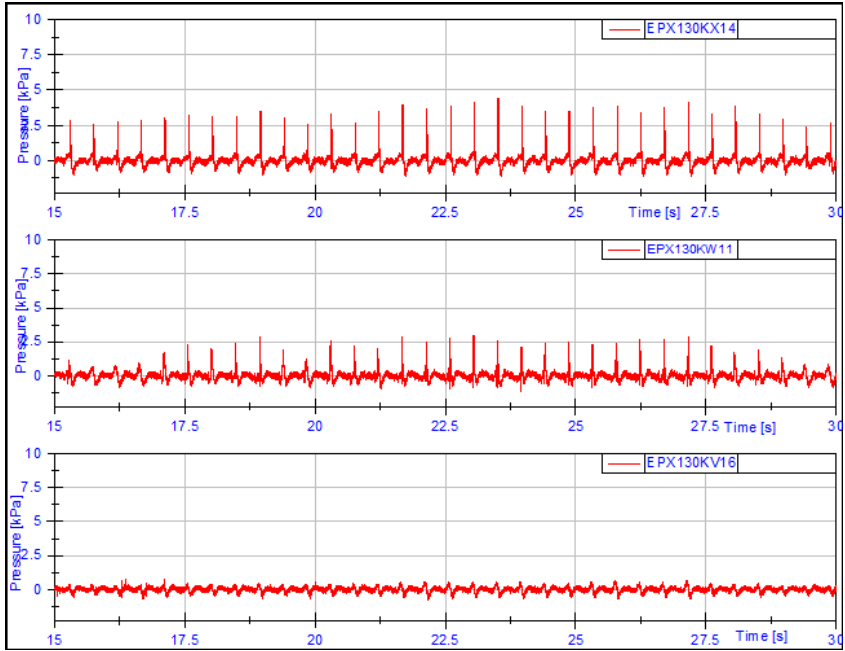


Figure A.24: Pressure trend for position Pos1 at Test 17

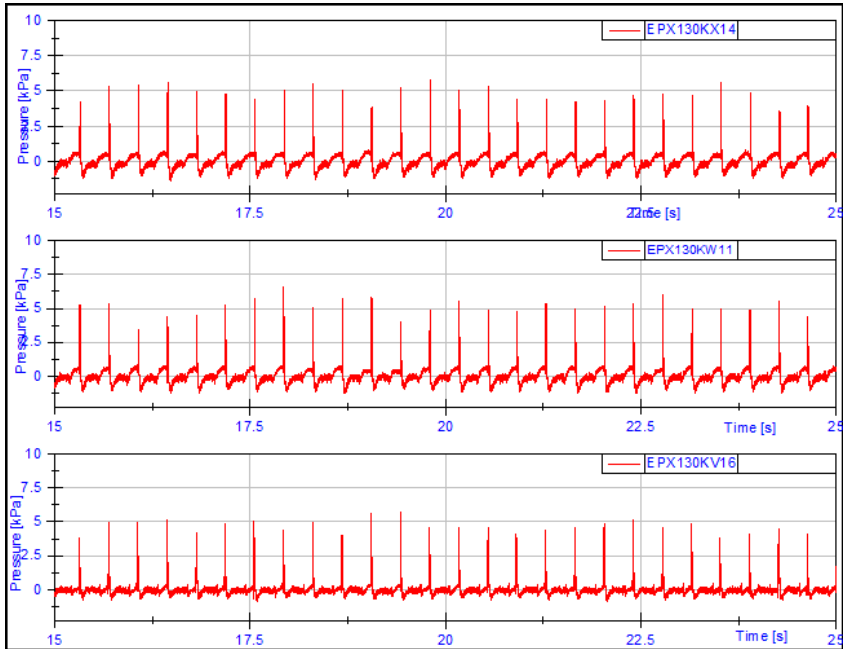


Figure A.25: Pressure trend for position Pos1 at Test 18

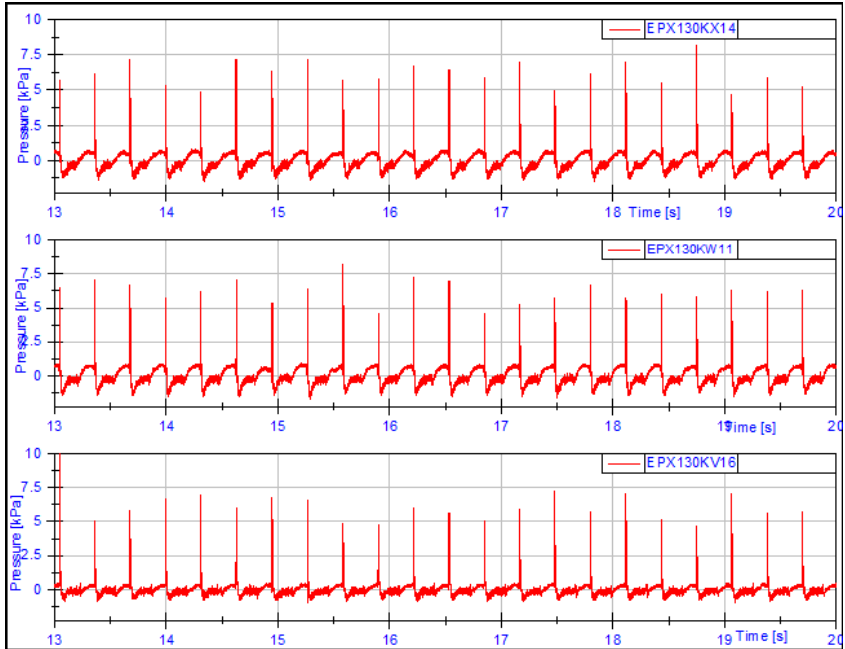


Figure A.26: Pressure trend for position Pos1 at Test 19

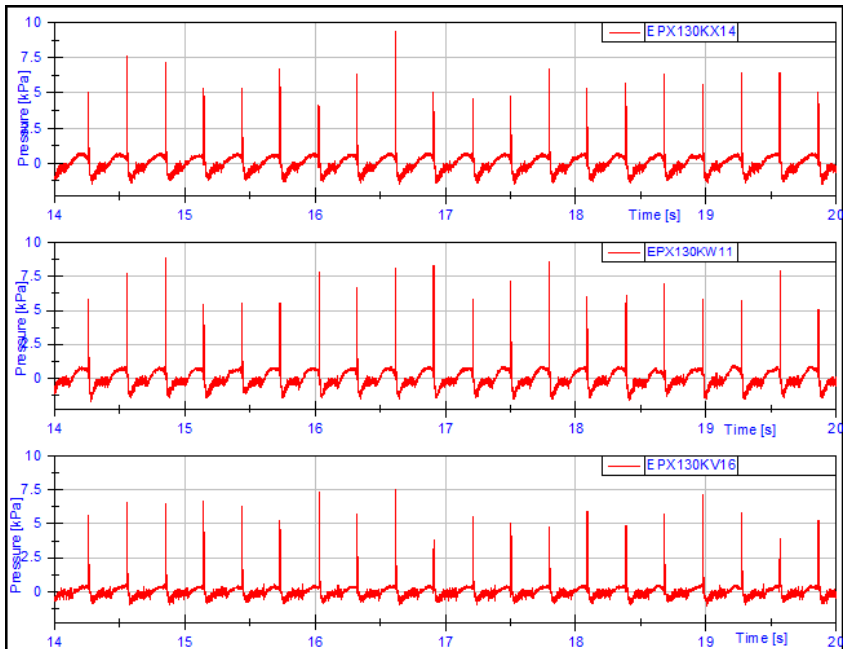


Figure A.27: Pressure trend for position Pos1 at Test 20

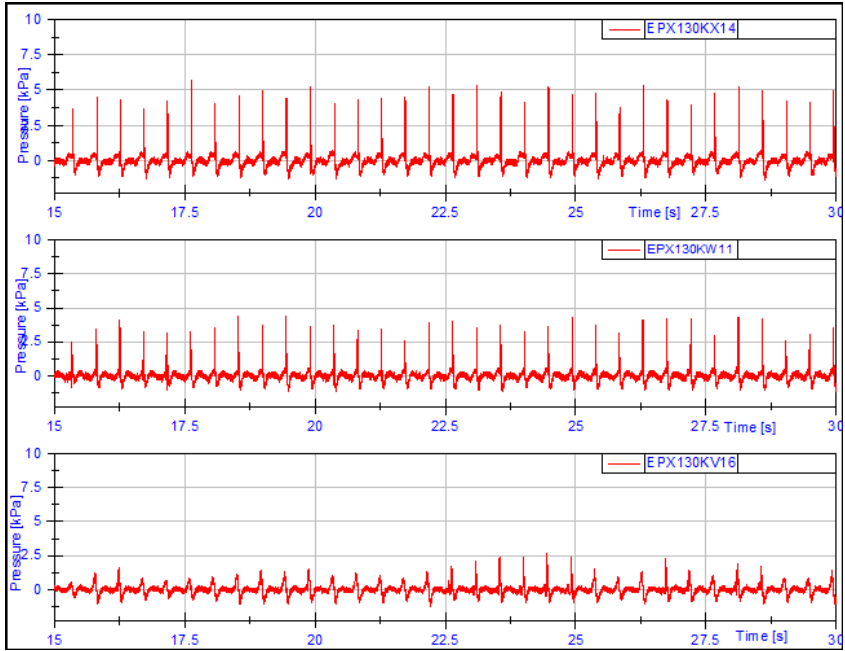


Figure A.28: Pressure trend for position Pos1 at Test 21

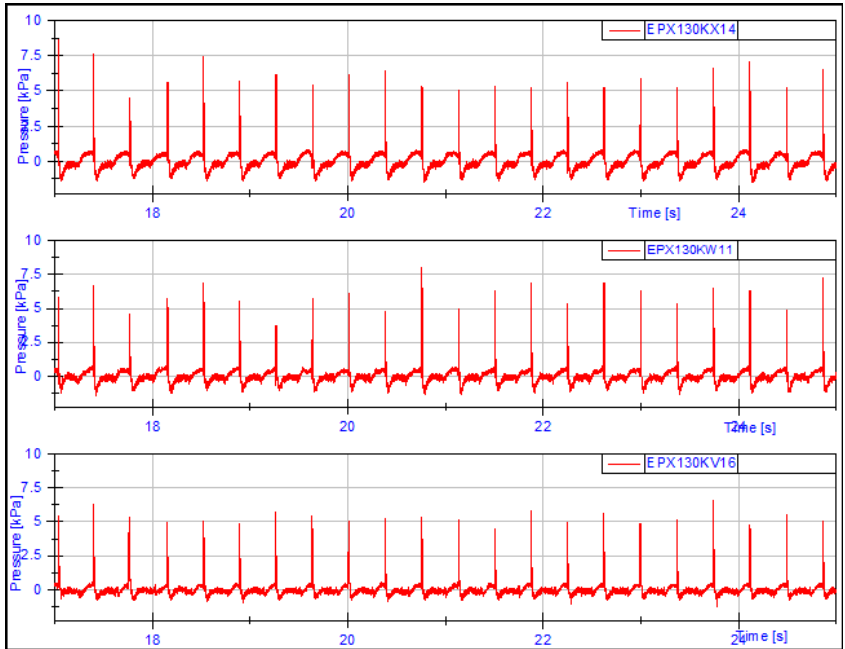


Figure A.29: Pressure trend for position Pos1 at Test 22

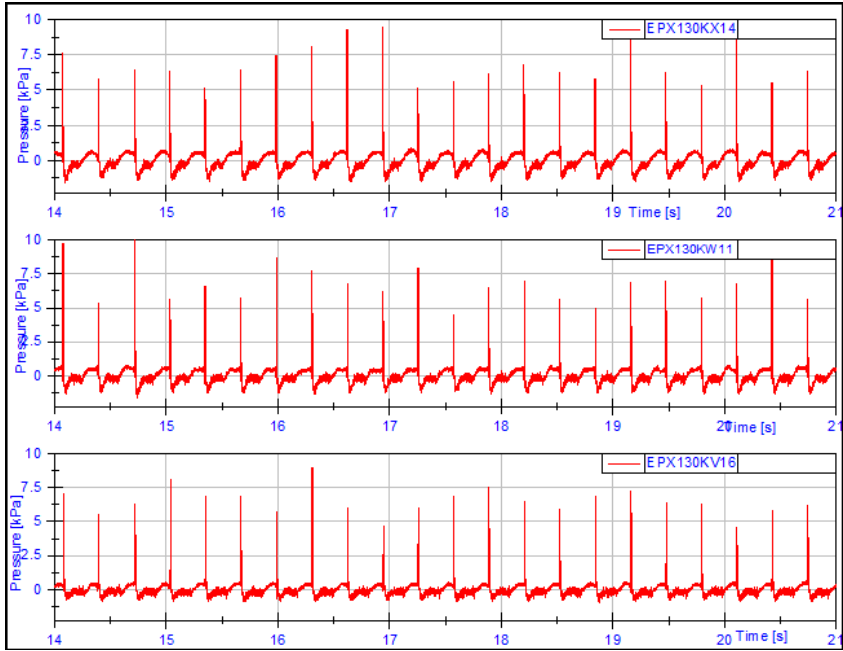


Figure A.30: Pressure trend for position Pos1 at Test 23

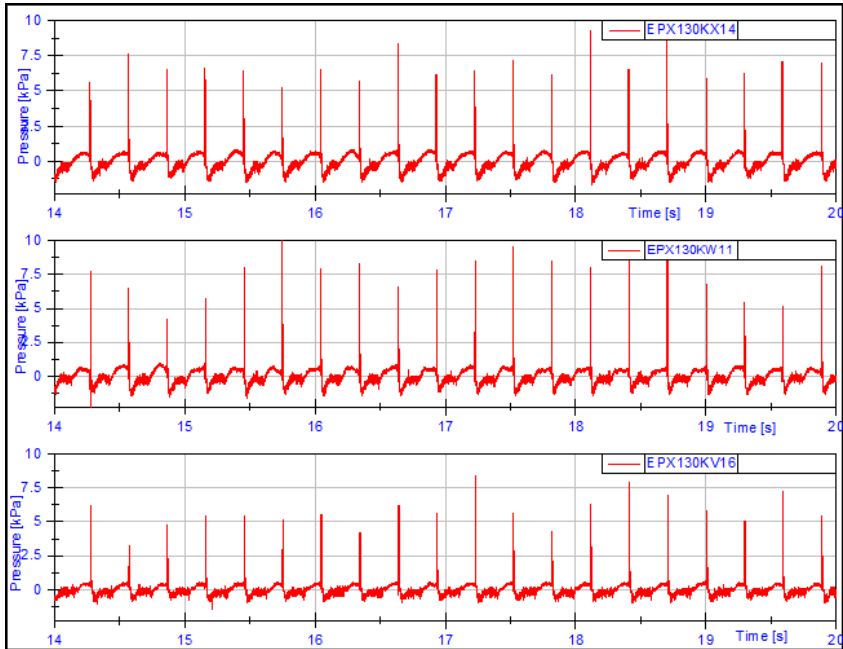


Figure A.31: Pressure trend for position Pos1 at Test 24

PART II

In the second part the diagrams of measured wave amplitude and vertical accelerations at the line 2 of points as well as represented in the Figure 2.5 are reported.

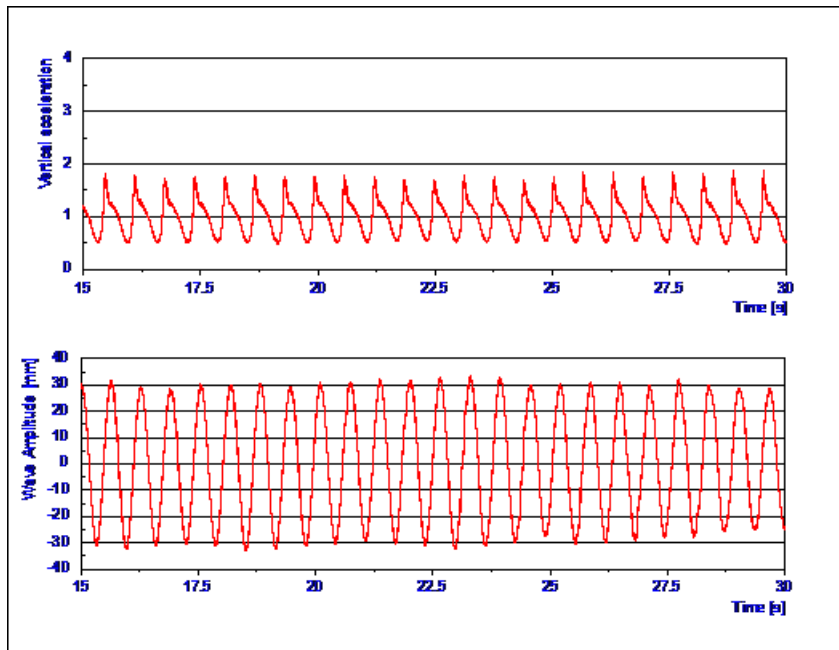


Figure A.32: Vertical accelerations and wave amplitude at model speed 3.4 m/s

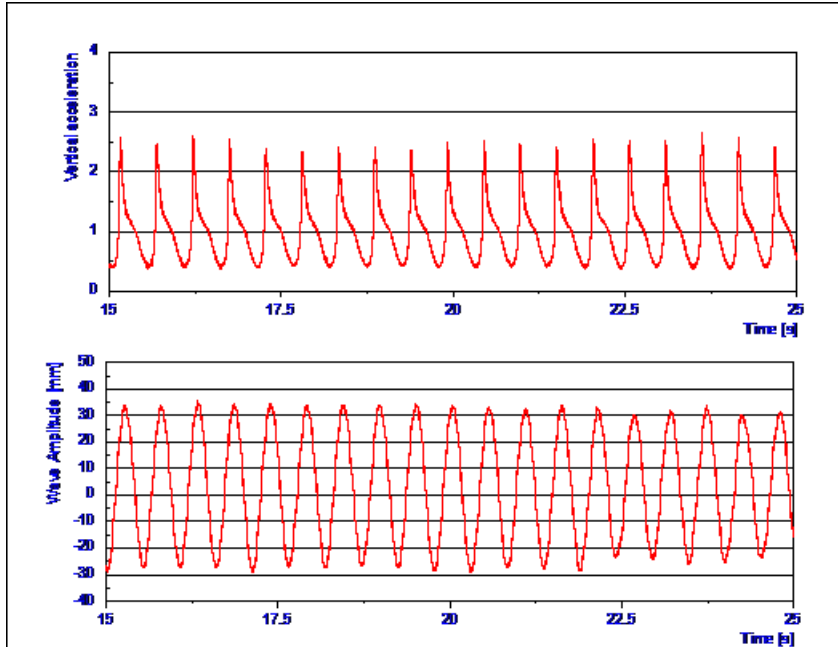


Figure A.33: Vertical accelerations and wave amplitude at model speed 4.6 m/s

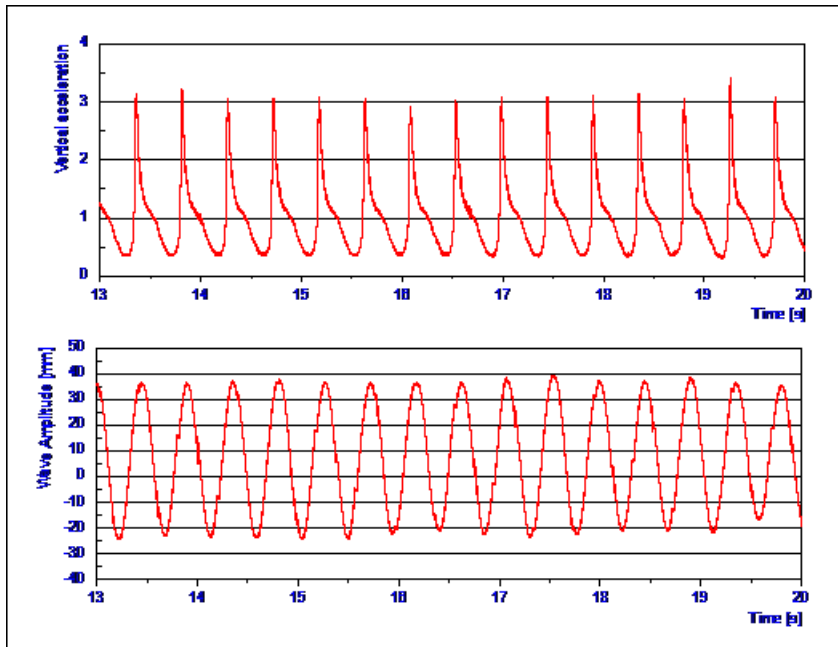


Figure A.34: Vertical accelerations and wave amplitude at model speed 5.75 m/s

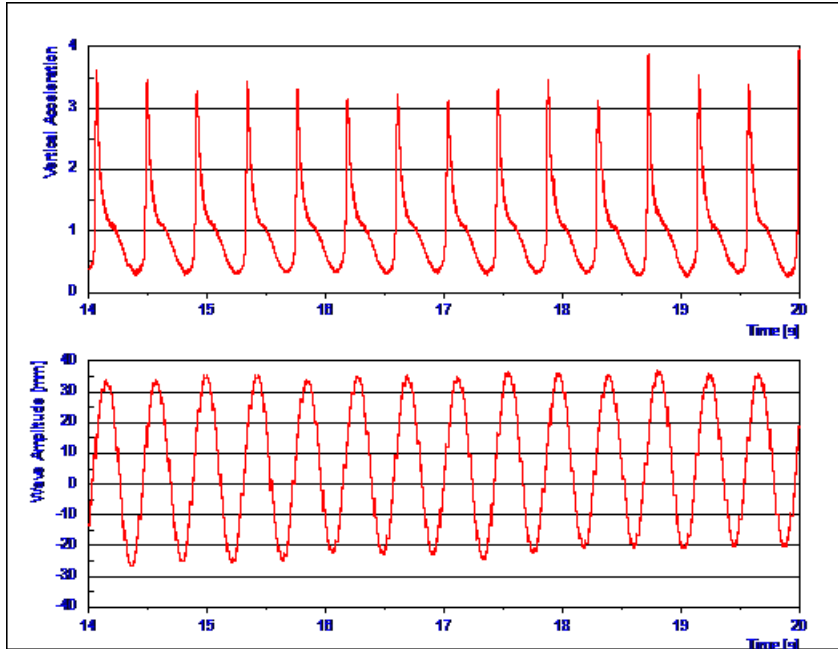


Figure A.35: Vertical accelerations and wave amplitude at model speed 6.32 m/s

APPENDIX B

PART I

In this part of appendix, the Fourier Transform of the pressure for every test speeds and for all points, is shown. The position of the measurement points, on the flat panel of bottom, is described in Figure 3.3 and Table 3.2.

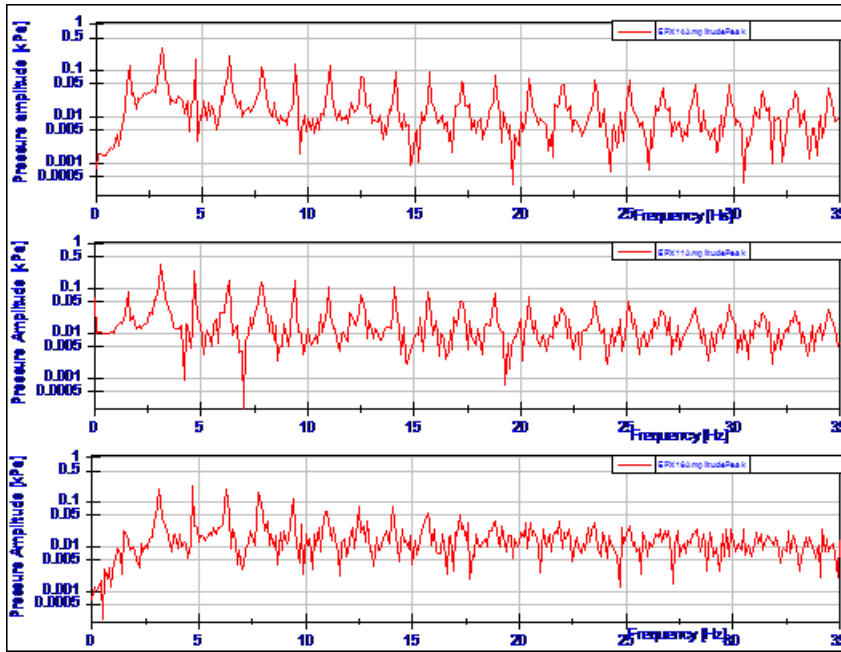


Figure B.1: Pressure FFT for position Pos1 at model speed 3.4 m/s

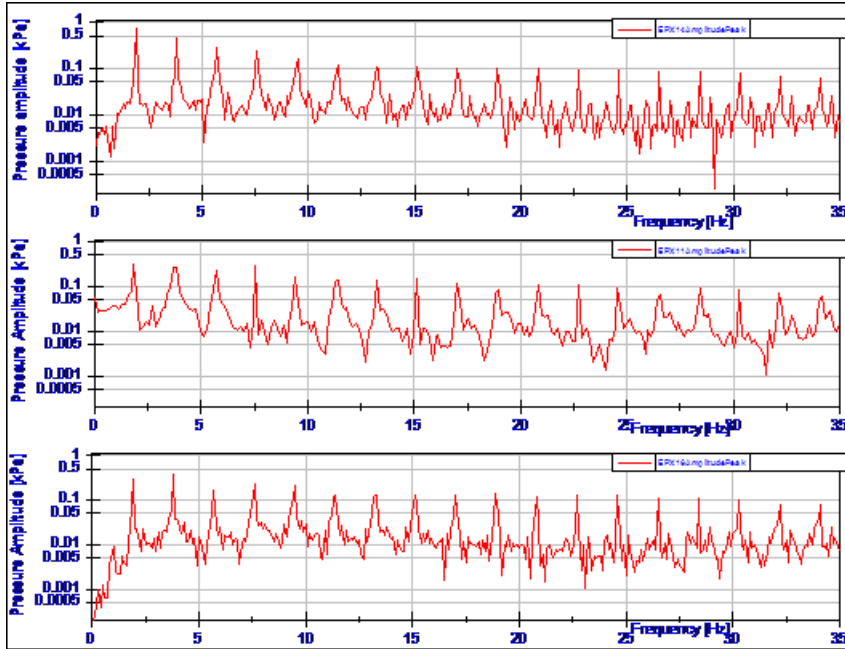


Figure B.2: Pressure FFT for position Pos1 at model speed 4.6 m/s

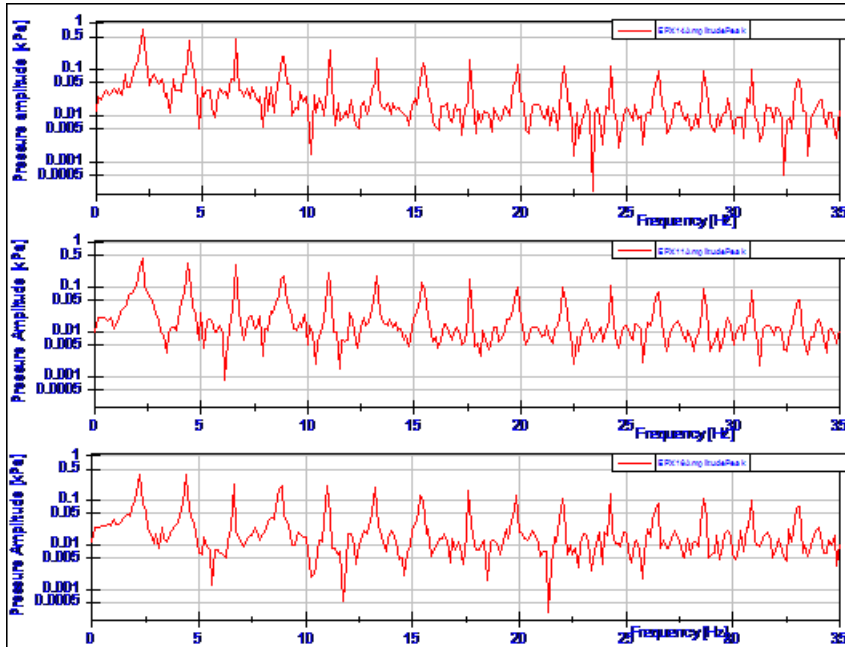


Figure B.3: Pressure FFT for position Pos1 at model speed 5.75 m/s

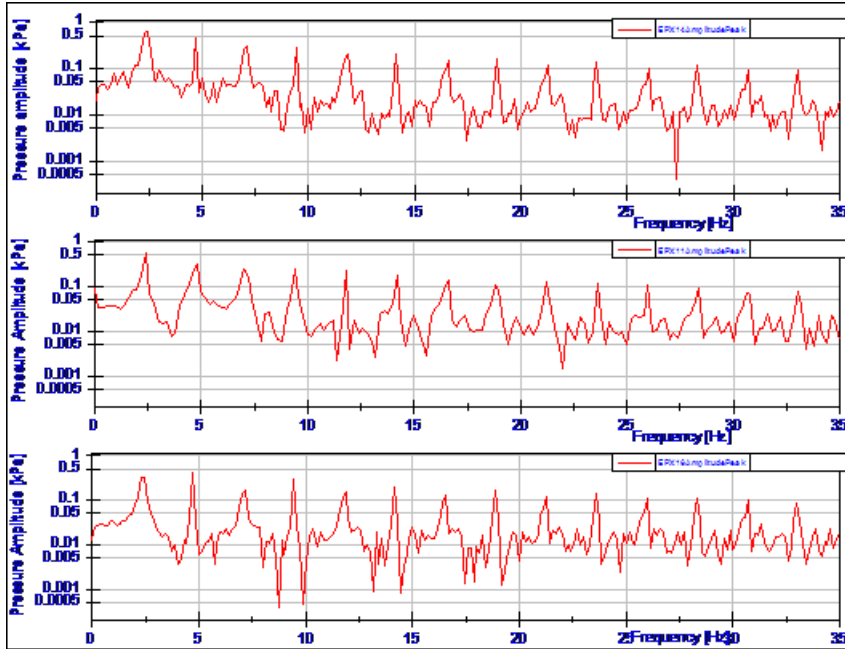


Figure B.4: Pressure FFT for position Pos1 at model speed 6.32 m/s

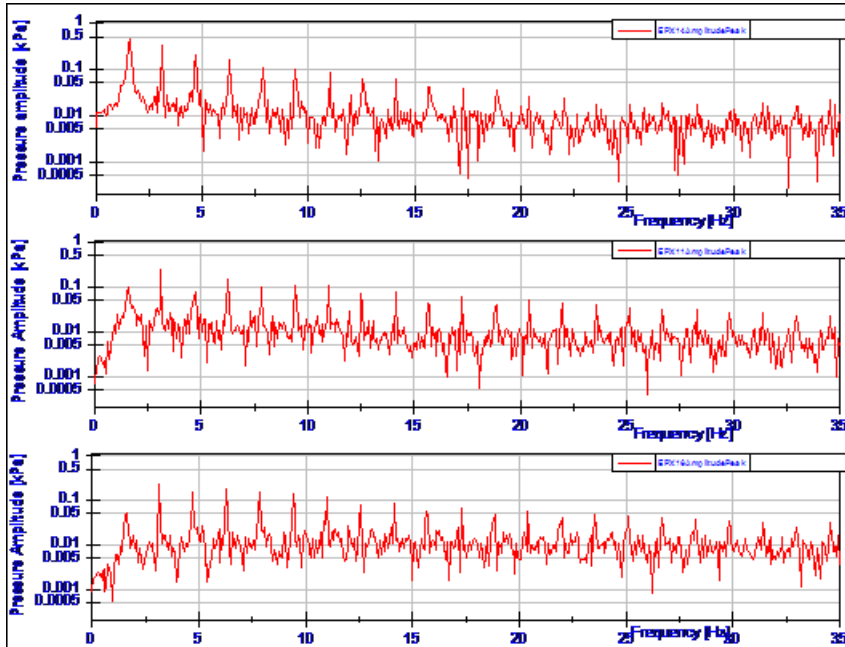


Figure B.5: Pressure FFT for position Pos2 at model speed 3.4 m/s

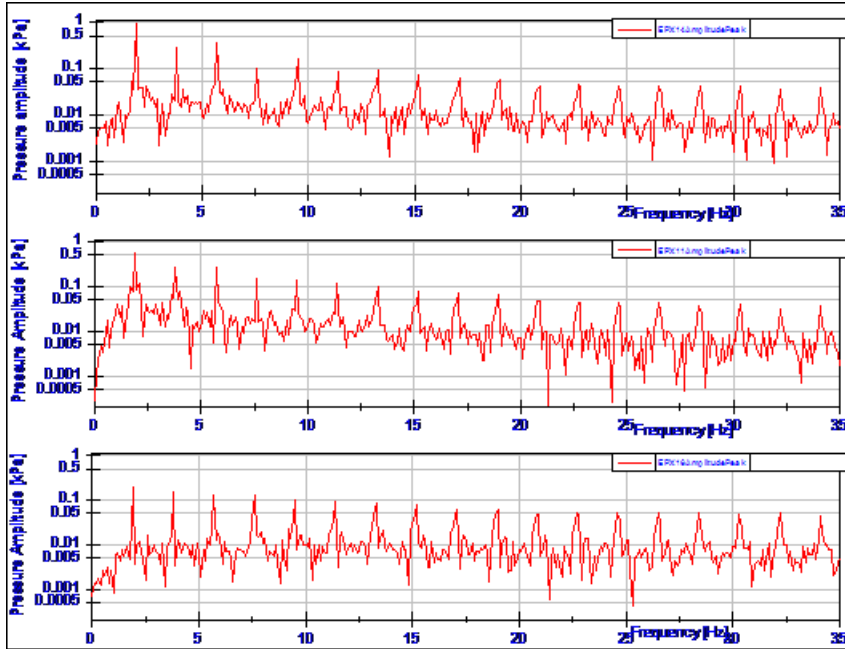


Figure B.6: Pressure FFT for position Pos2 at model speed 4.6 m/s

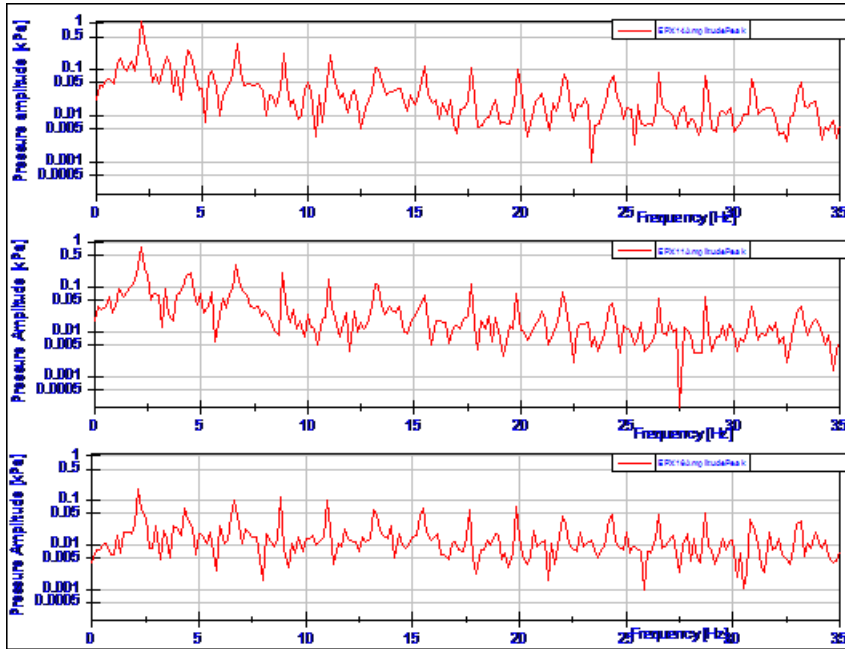


Figure B.7: Pressure FFT for position Pos2 at model speed 5.75 m/s

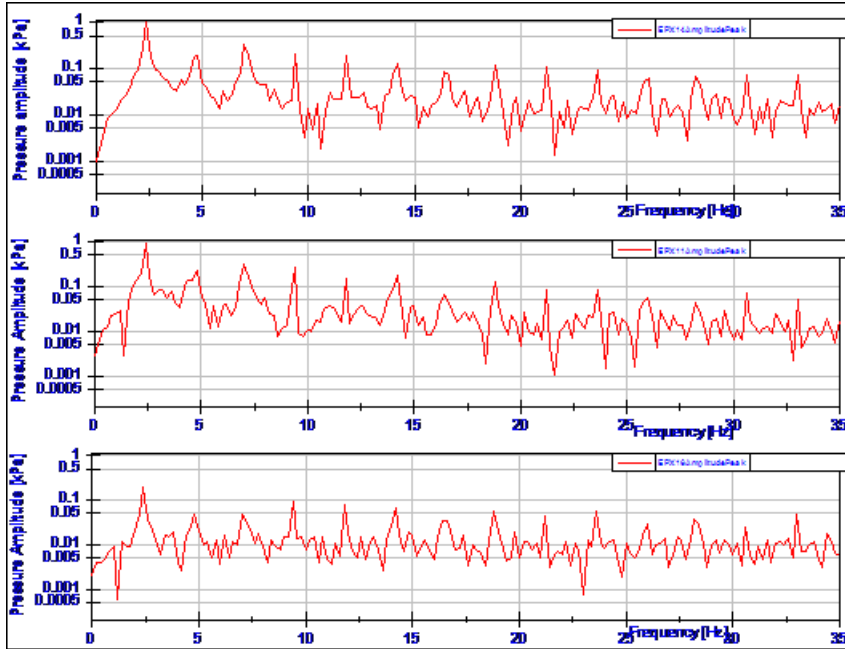


Figure B.8: Pressure FFT for position Pos2 at model speed 6.32 m/s

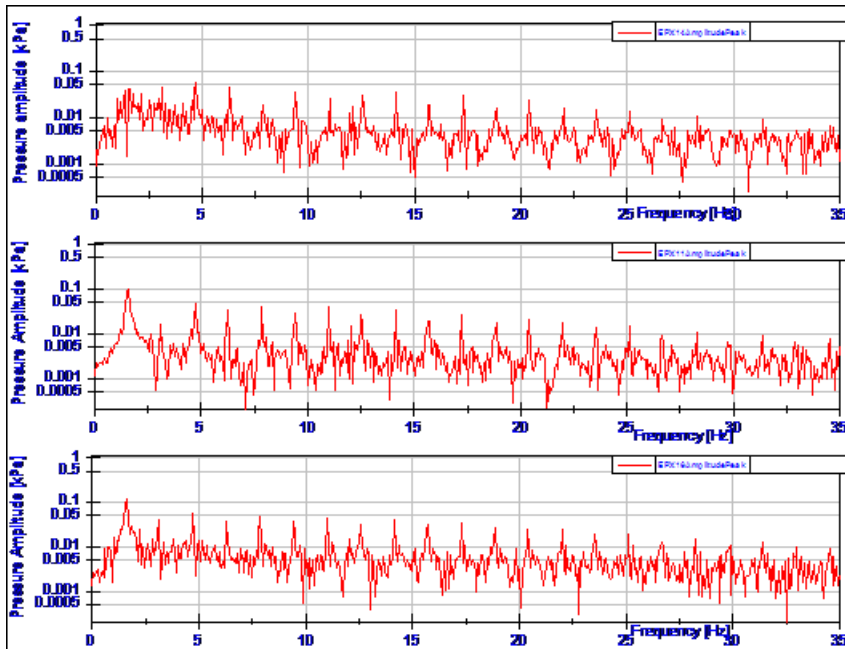


Figure B.9: Pressure FFT for position Pos3 at model speed 3.4 m/s

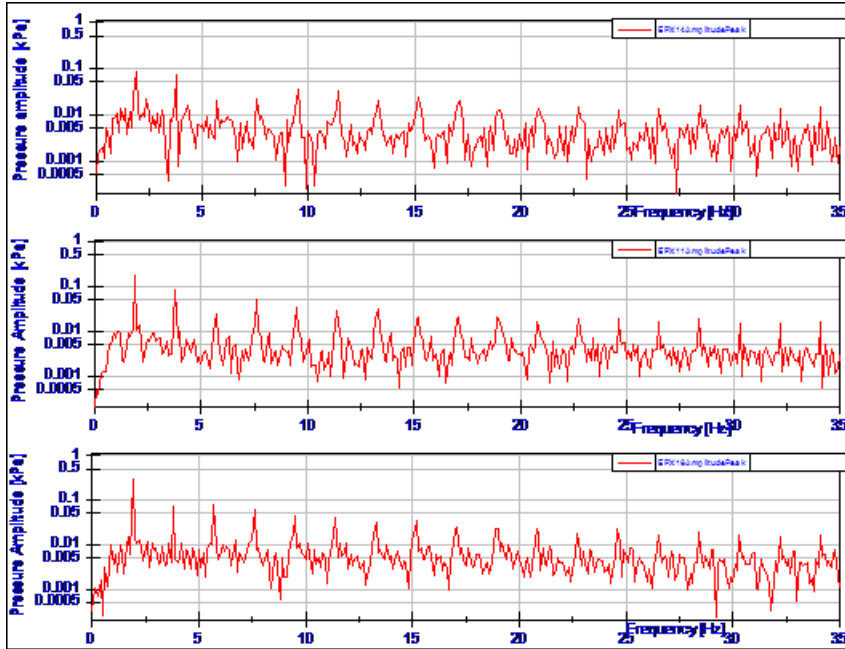


Figure B.10: Pressure FFT for position Pos3 at model speed 4.6 m/s

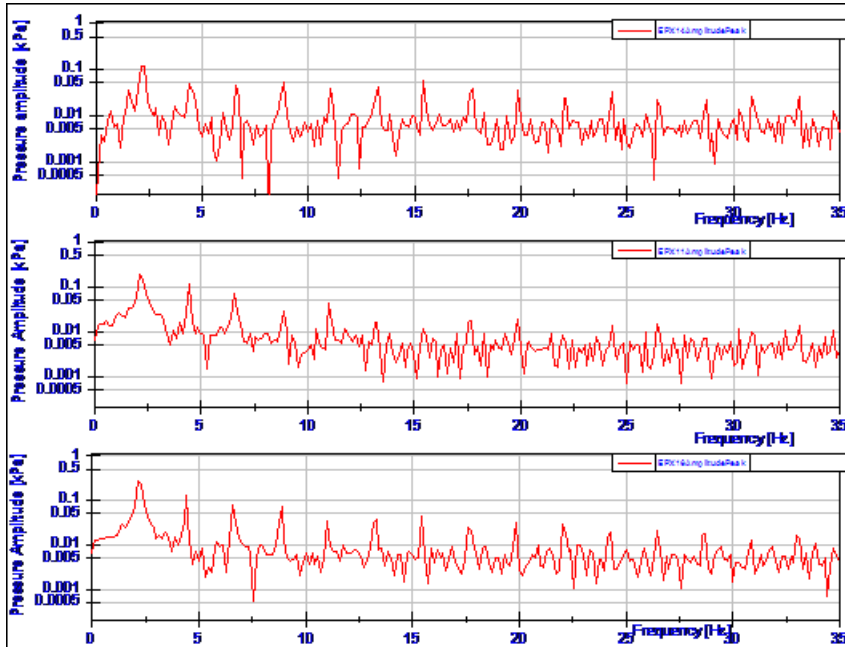


Figure B.11: Pressure FFT for position Pos3 at model speed 5.75 m/s

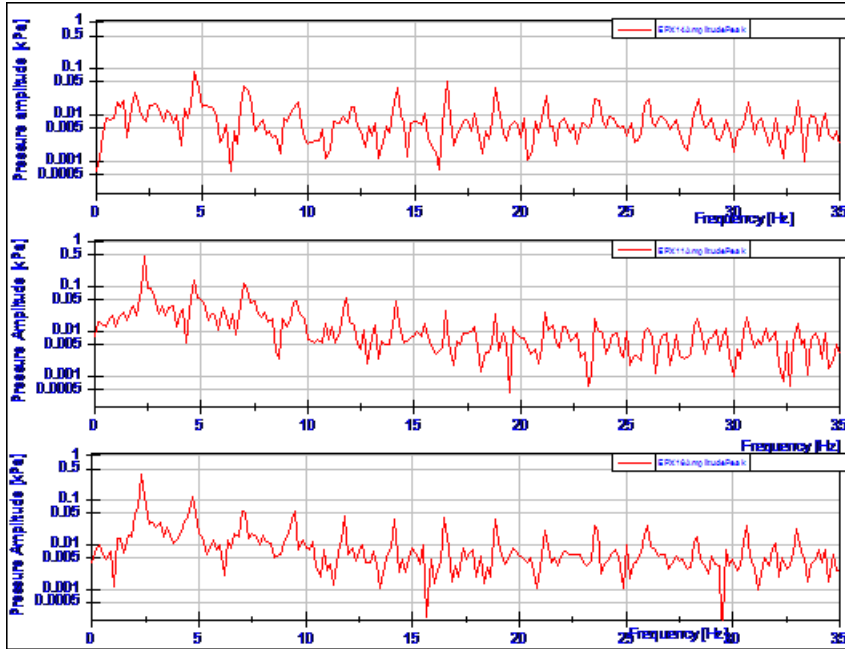


Figure B.12: Pressure FFT for position Pos3 at model speed 6.32 m/s

PART II

In the second part the FFT diagrams of measured wave amplitude and vertical accelerations at the line 1 of points as well as represented in the Figure 3.3, are presented

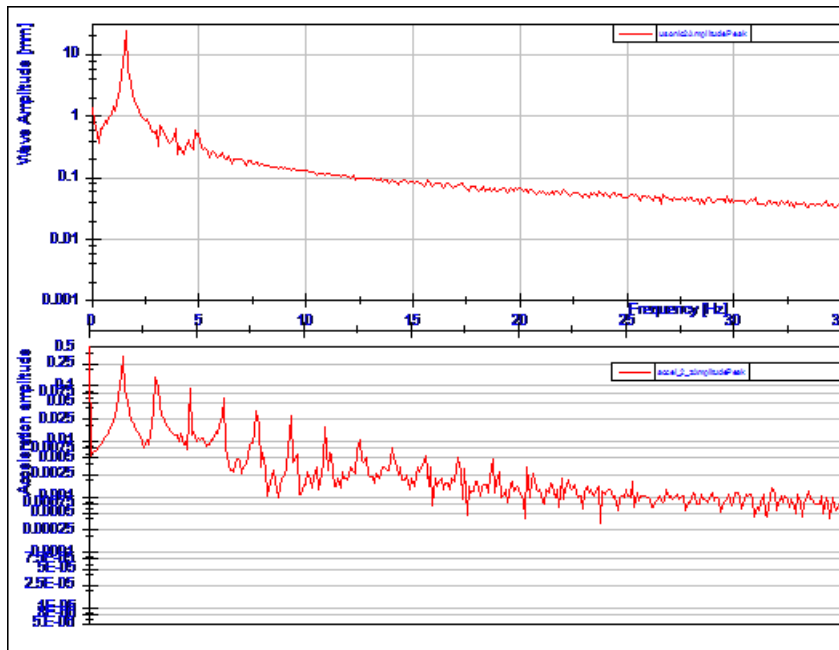


Figure B.13: FFT of vertical accelerations and wave amplitude at model speed 3.4 m/s

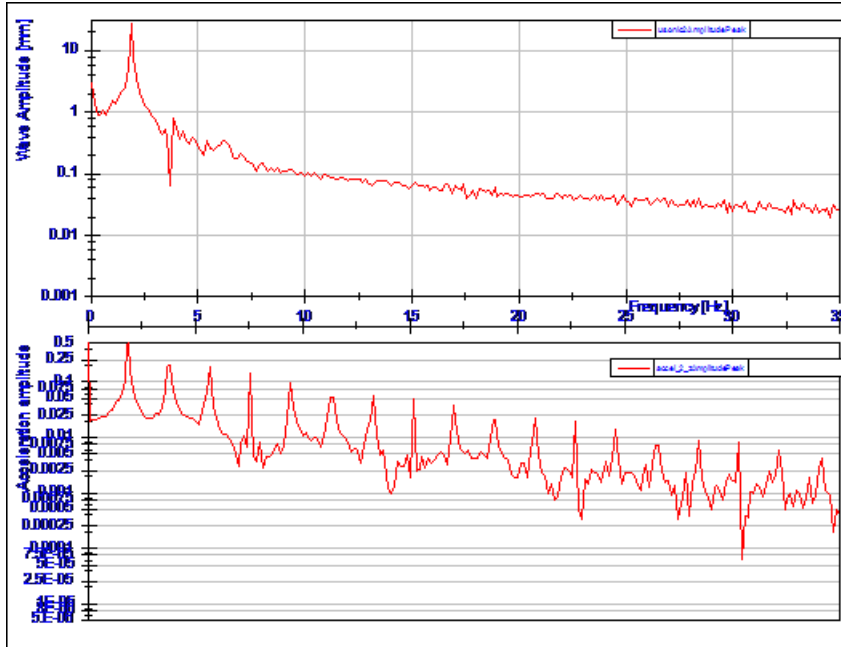


Figure B.14: FFT of vertical accelerations and wave amplitude at model speed 4.6 m/s

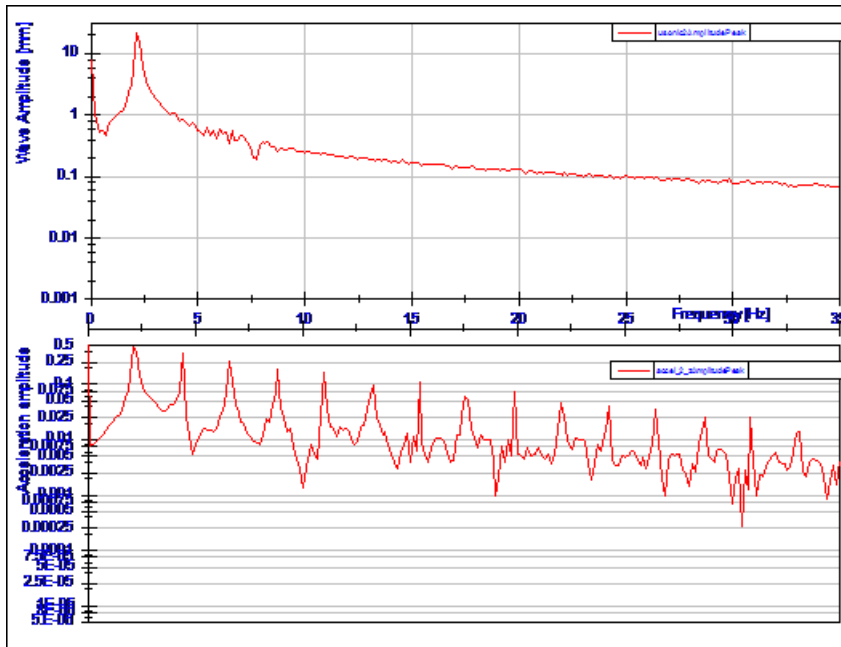


Figure B.15: FFT of vertical accelerations and wave amplitude at model speed 5.75 m/s

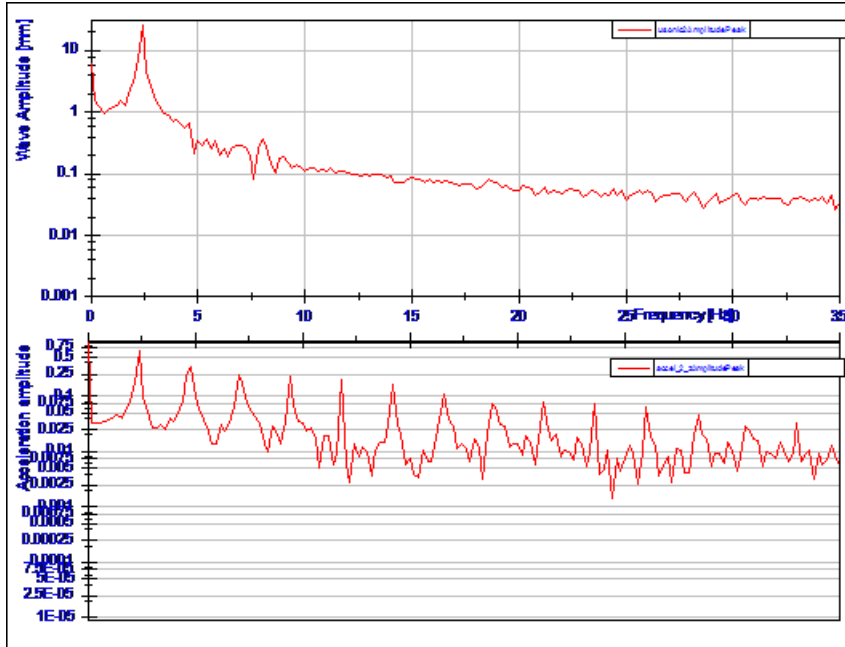


Figure B.16: FFT of vertical accelerations and wave amplitude at model speed 6.32 m/s

6. ACKNOWLEDGMENTS

Author would like to acknowledge all the staff of the "towing tank" of Department of Industrial Engineering of the University of Naples Federico II and Dr. A Bove for his important support to entire experimental campaign and instruments set up. Furthermore a huge acknowledgment to all Ph.D. tutors for their dedication to this project.

BIBLIOGRAPHY

- [1] A. S. Yigit and A. P. Christoforou, "Impact dynamics of composite beams," *Composite Structures*, vol. 32, pp. 187-195, 1995.
- [2] C. T. Sun, "An analytical method for evaluation of impact damage energy of laminated composites," presented at the Composite Materials: Testing and Design (fourth edition), Philadelphia, PA, 1977.
- [3] A. L. Dobyns, "Analysis of simply-supported orthotropic plates subject to static and dynamic loads," *AIAA Journal*, vol. 19, pp. 642-650, 1981.
- [4] S. H. Yang and C. T. Sun, "Indentation law for composite laminates," presented at the Composite Materials: Testing and Design (sixth edition), Philadelphia, PA, 1982.
- [5] M. Yang and P. Qiao, "Higher-order impact modeling of sandwich structures with flexible core," *International Journal of Solids and Structures*, vol. 42, pp. 5460-5490, 2005.
- [6] P. Qiao and M. Yang, "Impact analysis of fiber reinforced polymer honeycomb composite sandwich beams," *Composite Part B*, vol. 38, pp. 739-750, 10 Mar 2006 2007.
- [7] T. V. Karman, "The impact of seaplane floats during landing," *NACA*, vol. Tech. note no. 321, 1929.
- [8] J. D. Wagner, "Landing of seaplanes," *National Advisory Committee for Aeronautics*, vol. TN 622, 1932.
- [9] R. Zhao and O. Faltinsen, "Water entry of two-dimensional bodies," *Journal of Fluid Mechanics*, vol. 246, pp. 593-612, 1993.
- [10] R. Zhao, *et al.*, "Water Entry of Arbitrary Two-Dimensional Sections with and without Flow Separation," presented at the Twenty-First Symposium on Naval Hydrodynamics, 1997.
- [11] O. M. Faltinsen, Ed., *Hydrodynamics of High-Speed Marine Vehicles*. 2005, p.^pp. Pages.
- [12] S. G. Lewis, *et al.*, "Impact of free-falling wedge with water: synchronized visualization, pressure and acceleration measurements," *Fluid Dynamics Research*, vol. 42, pp. 1-30, 16 March 2010 2010.
- [13] E. Ciappi, "Impact of rigid and elastic structures on the water surface," Ph. D. in Meccanica teorica e applicata, Dipartimento di Meccanica e Aeronautica, La Sapienza, Roma.

- [14] A. Carcaterra and E. Ciappi, "Hydrodynamic shock of elastic structures impacting on the water: theory and experiments," *Journal of Sound and Vibration*, vol. 271, pp. 411-439, 2004.
- [15] X. Mei, *et al.*, "On the water impact of general two-dimensional sections," *Applied Ocean Research*, vol. 21, pp. 1-15, 1999.
- [16] O. A. Hermundstad and T. Moan, "Efficient calculation of slamming pressures on ships in irregular seas," *Journal of Marine Science and Technology*, vol. 12, pp. 160-182, 2007.
- [17] O. A. Hermundstad and T. Moan, "Practical calculation of slamming pressures in irregular oblique seas," presented at the International Conference on Fast Sea Transportation, Athens, Greece, 2009.
- [18] I. Stenius and A. Rosén, "FE - Modelling of hydrodynamic hull-water impact loads," presented at the 6th European LS-DYNA Users' Conference.
- [19] K. Das and R. C. Batra, "Local water slamming impact on sandwich composite hulls," *Journal of Fluids and Structures*, vol. 27, pp. 523-551, 2011.
- [20] Sumitoshi Mizoguchi and K. Tanizawa, "Impact Wave Loads due to Slamming { A Review," *Ship Technology Research*, vol. 43, 1996.
- [21] S. P. Kim, *et al.*, "Slamming impact design loads on large high speed naval craft," presented at the International Conference on innovative approaches to further increase speed of fast marine vehicles, moving above, under and in water surface, Saint-Petersburg, Russia, 2008.
- [22] M. Battley and D. Svensson, "Dynamic response of marine composites to slamming loads," ed. Engineering Dynamics Department, Industrial Research Limited - Auckland, New Zealand, 2001.
- [23] G. J. Simitzes, *et al.*, "Structural Similitude and Scaling Laws for Plates and Shells: A Review
Advances in the Mechanics of Plates and Shells." vol. 88, D. Durban, *et al.*, Eds., ed: Springer Netherlands, 2002, pp. 295-310.
- [24] G. J. Simitzes and J. Rezaeepazhand, "Title," unpublished|.
- [25] P. W. Bridgman, *Dimensional Analysis*, II ed. New Haven - Yale University, 1931.
- [26] A. A. Sonin, "Title," unpublished|.
- [27] E. O. Macagno, "Historico-critical review of dimensional analysis," *Journal of the Franklin Institute*, vol. 292, pp. 391-402, 1971.

- [28] E. Buckingham, "On Physically similar systems illustrations of the use of dimensional equations," *Physics Reviews*, vol. IV, pp. 345-376, 1914.
- [29] June Lee and P. A. Wilson, "Experimental study of the hydro-impact of slamming in a modern racing sailboat," *Journal of Sailboat Technology*, 26-08-2009 2010.
- [30] P. Manganelli, *et al.*, "Investigation of slamming loads using slam patches on a scale model of an open 60' class yacht," presented at the The international HISWA Symposium on yacht design and yacht construction, 2002.
- [31] M. Battley, *et al.*, "Structural Responses of High Performance Sailing Yachts to Slamming Loads," presented at the 11th International Conference on Fast Sea Transportation, Honolulu, Hawaii, USA, 2011.
- [32] M. Battley and T. Allen, "Dynamic performance of marine sandwich panel structures," presented at the 18th International Conference on composite materials, 2011.
- [33] M. Battley and T. Allen, "Servo-hydraulic System for Controlled Velocity Water Impact of Marine Sandwich Panels," *Experimental Mechanics*, vol. 52, pp. 95-106, 29 August 2011 2012.
- [34] M. Battley, *et al.*, "Effects of panels stiffness on slamming responses of composite hull panels," ed. Centre for Advanced Composite Materials, University of Auckland, 2009.
- [35] K. Garne, "Modeling of planing craft in waves," ed, 2004.
- [36] K. Garne, *et al.*, "In Detail Investigation of planing pressure," presented at the HYDRALAB III, Hannover, 2010.
- [37] L. Sebastiani, *et al.*, "A Theoretical / Experimental investigation of the slamming pressures on fast monohull vessels," presented at the FAST 2001, Southampton, UK, 2001.
- [38] J.-M. Rousset, *et al.*, "Slamming experiments on a ship model," ed.
- [39] E. Begovic and C. Bertorello, "Resistance assessment of warped hullform," *Ocean Engineering* vol. 56, pp. 28 - 42 2012.
- [40] E. Begovic, *et al.*, "Experimental Seakeeping Assessment of Warped Planing Hull," *Ocean Engineering*, vol. 83, pp. 1-15, 1 June 2014 2014.
- [41] R. D. Blevins, Ed., *Formula for natural frequency and mode shape*. Malabar, Florida: Robert E. Krieger Publishing Company, 1979, p.^pp. Pages.